JCTC Journal of Chemical Theory and Computation

pubs.acs.org/JCTC Article

A Quadratic Pair Atomic Resolution of the Identity Based SOS-AO-MP2 Algorithm Using Slater Type Orbitals

Arno Förster,* Mirko Franchini, Erik van Lenthe, and Lucas Visscher

Cite This: J. Chem. Theory Comput. 2020, 16, 875−891

Read Online

ACCESS | Metrics & More | Article Recommendations | Supporting Information

ABSTRACT: We report a production level implementation of pair atomic resolution of the identity (PARI) based second-order Møller−Plesset perturbation theory (MP2) in the Slater type orbital (STO) based Amsterdam Density Functional (ADF) code. As demonstrated by systematic benchmarks, dimerization and isomerization energies obtained with our code using STO basis sets of triple-ζ-quality show mean absolute deviations from Gaussian type orbital, canonical, basis set limit extrapolated, global density fitting (DF)-MP2 results of less than 1 kcal/mol. Furthermore, we introduce a quadratic scaling atomic orbital based spin-opposite-scaled (SOS)-MP2 approach with a very small prefactor. Due to a worst-case scaling of $O(N^3)$, our implementation is very fast already for small systems and shows an exceptionally early crossover to canonical SOS-PARI-MP2. We report computational wall time results for linear as well as for realistic three-dimensional molecules and show that triple-ζ quality calculations on molecules of several hundreds of atoms are only a matter of a few hours on a single compute node, the bottleneck of the computations being the SCF rather than the post-SCF energy correction.

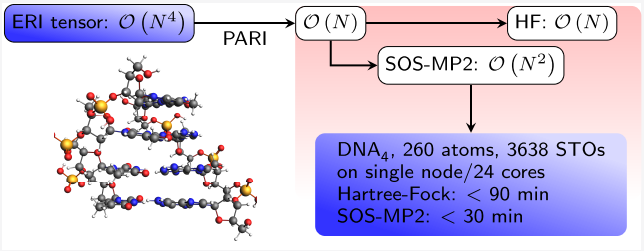

1. INTRODUCTION

Spurred by the interest in large biomolecules and inorganic systems, the last decades have witnessed a tremendous effort in making accurate electronic structure methods routinely applicable to molecules and solids of ever increasing size. Due to its still unrivaled price/performance-ratio,[1] Kohn−Sham (KS)[2] density functional theory (DFT)[3,4] has established itself as the workhorse of quantum chemistry for medium and large systems.[5−11] Unfortunately, due to an insufficient description of electron correlation, state of the art semilocal[12] or hybrid[13] approximations to the exact exchange−correlation functional often fail to accurately account for London dispersion-type effects[14−18] and noncovalent interactions.[19] Both are of paramount importance for a thorough understanding of the properties and reactivity of biochemical systems and organometallic compounds.[20,21]

Wave function based *ab initio* methods, however, offer a systematic route toward the complete and explicit description of all dynamical correlation effects. As known only too well, this does not come for free: Expressed in terms of canonical orbitals, their steep computational scaling (N^5 (N is a measure for the system size[22]) for second-order Møller−Plesset perturbation theory (MP2),[23] N^6 for CC with singles and doubles excitations (CCSD),[24−26] N^7 for CCSD with a perturbative treatment of triple excitations (CCSD(T)),[27] respectively), their tremendous memory requirements in practical implementations,[28] and their slow convergence to the basis set-limit[29] complicate the application of these methods to large molecular systems.

The commonly realized concept of the locality of dynamical electron correlation has led to a family of low-scaling wave function based methods approaching the accuracy of their canonical counterparts. The field came to life when Pulay, Saebø, and co-workers employed localized molecular orbitals (MO)[30−36] and restricted excitations to local domains in configuration interaction (CI)[37,38] and MPn[39−41] computations. Successfully transferred to the realms of highly accurate CC theory by Werner and co-workers,[42] a plethora of low-scaling CC[43−49] and MP2[51−55] codes has been developed. With the size of the excitation domains becoming a liming factor, Neese and co-workers[28,56−59] and others[60−69] revived the decades ago developed[70−83] pair natural orbital (PNO)[84,85] approach to further compress the virtual subspaces. At the same time, relying on a physical partition of the system of interest instead of the orbital space, several flavors of fragment based approaches have been brought forward. Most notably these are the incremental method,[86−88] the cluster-in-molecule,[89−91] the divide-and-conquer,[92−98] and the divide-expand-consolidate[99−106] approaches.

Received: August 27, 2019
Published: January 13, 2020

https://dx.doi.org/10.1021/acs.jctc.9b00854
J. Chem. Theory Comput. 2020, 16, 875−891

While having greatly extended the range of computationally tractable molecules,[58,68,69,107] local CC methods can still not compete with the wall clock times of KS-DFT computations on the hybrid level. This is not necessarily the case for MP2.[59,65,67] Although less accurate than CCSD and higher CC methods, MP2 has been demonstrated to accurately describe properties such as dispersion interactions and hydrogen binding,[18,108,109] NMR chemical shifts,[110] and polarizabilities[111,112] as well as molecular interaction energies[113] and conformational energies,[114] especially in its spin-scaled variants.[115−118] Furthermore, MP2 energies from KS orbitals have been used extensively to incorporate explicit electron correlation effects into the calculation of KS-DFT energies.[119−125] These so-called double hybrid (DH) density functionals often yield clear improvements over hybrid functionals,[126,127] making low-cost MP2 implementations extremely desirable.

While a simple expression for the MP2 amplitudes exists using canonical orbitals, the MP2 amplitude equations can only be solved iteratively in most fragments, as well as localized orbital based formalisms (the integral-direct formulation of Nagy et al.[67,91] should be mentioned as a prominent exception). Retaining the simplicity of the canonical formalism, exploiting sparsity in the electron-repulsion integral (ERI) tensor[128] instead is yet another alley toward the order-N computation of MP2 energies. Formally quartically scaling, it is well-known that the number of nonzero elements in the ERI tensor only scales linearly with system size. The resolution of the identity (RI) or density fitting approximation (DF)[129−140] is the most popular technique to overcome the scaling of the fourth-order ERI tensor by decomposing it into third-order and second-order tensors and has been applied successfully to reduce the prefactor of canonical MP2.[48,105,106,141−149]

Reformulating the energy denominator of canonical MP2 as an integral expression[150−152] (often referred to as a Laplace transform (LT)), the MP2 energy can be evaluated in the atomic orbital (AO) basis. In this representation, approaches to reduce the dimensionality of the ERI tensor can be applied more efficiently. Using integral prescreening techniques,[152−156] reduced-scaling AO-MP2 codes could be realized by Ayala and Scuseria,[157,158] Ochsenfeld and co-workers,[50,159−162] and others.[163] However, employing large sets of spatially extended AOs, the prefactor of these methods is increased significantly due to an increase of linear dependencies in the pseudo density matrices (PDM).[160,164] Cholesky decomposition (CD) based techniques[165−169] can be used to obtain a set of localized occupied (virtual) orbitals with cardinality equal to the rank of the occupied (virtual) PDMs. Employing this approach in conjunction with screening techniques and DF, very fast AO-MP2 implementations have been reported by the Ochsenfeld group.[164,170−173] Also the tensor hypercontraction (THC) approach to compress the ERI tensor, brought forward by Martínez and co-workers,[174−178] has been used successfully to obtain fast and reliable low-scaling MP2 implementations.[174,179−181]

In this work, we explore the use of the pair atomic resolution of the identity (PARI)[129,182−187] in the evaluation of MP2 energies. In this approach, the cubic scaling of global DF is reduced automatically by expanding products of AO pairs in terms of fit functions centered on the same atoms as the pair of target functions only. In this way, the complexity of the ERI tensor only scales quadratically with system size and linearly when insignificant pairs of basis functions are neglected. Already developed as early as in the 1970s by Baerends et al.,[129] its potential to accelerate the evaluation of the exact exchange has only been demonstrated recently.[183,185−188] Although some concerns regarding its accuracy and numerical stability have been brought forward,[183,189] the applicability of the PARI approximation in the framework of MP2 and the random phase approximation (RPA) has been reported by Ihrig et al.[186]

The purpose of this paper is 2-fold. First, we present a production level implementation of PARI based MP2 (PARI-MP2) using STOs. By means of systematic benchmarks on various test sets, we demonstrate that our PARI-MP2 implementation in conjunction with triple-ζ quality basis set[190] reproduces the basis set limit of canonical MP2 within less than 1 kcal/mol on average. Second, we show how the PARI approach can be used to considerably speed up the evaluation of MP2 energies in a memory efficient way. As we think that these are the most realistic targets for local correlation methods, we explicitly focused on designing an algorithm which is very fast and reliable for small as well as medium, compact systems of up to several hundreds of atoms: We herein report a quadratic scaling AO based spin-opposite-scaled (SOS)-PARI-MP2 implementation of order-N^3 without any distance effects considered. Due to a small prefactor, the computation of the SOS-MP2 energy is much faster than the SCF itself. Although we herein refer often to STO basis sets, we emphasize that our approach is completely general and can be implemented with basis sets of arbitrary type.

This paper is organized as follows: In section 2, we introduce the PARI approach to evaluate the exact exchange and describe our AO based SOS-PARI-MP2 implementation (SOS-AO-PARI-MP2 in the following). In section 3, we report our benchmark results and demonstrate the excellent scaling properties of our algorithm for selected medium and large molecules. Finally, in section 4 we summarize and conclude this work.

The herein frequently appearing indices are summarized as follows:

- A, B, C, D: indices denoting atomic centers, where $A = 1, ..., N_a$ and N_a denotes the number of atoms in the system.
- $\mu, \nu, \kappa, \lambda$: AO basis indices, where $\mu = 1, ..., N_b^A$, where N_b^A denotes the number of basis functions N_b centered on atom A.
- $\alpha, \beta, \gamma, \delta$: auxiliary basis indices, where $\alpha = 1, ..., N_f^A$, and N_f^A is the number of auxiliary fit functions N_f centered on atom A.
- The following convention is always applied: $\mu, \alpha \in A$, $\nu, \beta \in B$, $\kappa, \gamma \in C$, $\lambda, \delta \in D$, which means that the indices μ,α always imply that the corresponding functions are centered on atom A.
- $\tilde{\mu}$ ($\tilde{\alpha}$) denote global AO basis indices (global auxiliary basis indices), ranging from 1 to $N_{b,all}$ ($N_{f,all}$), where $N_{b,all}$ ($N_{f,all}$) are the number of AOs (auxiliary fit functions) of the whole system.
- τ: Numerical quadrature point indices, ranging from 1 to N_{nq}, where N_{nq} denotes the number of quadrature points.

2. THEORY

2.1. Pair Atomic Resolution of the Identity for the Exact Exchange. PARI (or local pair fitting) is a quite

https://dx.doi.org/10.1021/acs.jctc.9b00854
J. Chem. Theory Comput. 2020, 16, 875−891

extreme variant of the more general local domain fitting approach. The general idea is to overcome the cubic scaling of global, Coulomb metric based DF using fit functions in the neighborhood of the target product only. When pair-atomic densities are chosen as local fitting domains, the PARI method is obtained. This approach is clearly more approximate than global DF but can be physically motivated as atom-centered basis functions generate strongly localized contributions to the total density; i.e., the AO pair density products $\chi_\mu(\mathbf{r})\,\chi_\nu(\mathbf{r}) \equiv \rho_{\mu\nu}$ are local in nature. Here, we only recapitulate shortly the concepts which are necessary to understand our MP2 implementation. We are planning to elaborate on our PARI-HF implementation in a forthcoming publication.

Each atomic pair density with AOs centered on a certain pair of atoms (A,B) is expanded in a local set of fit functions $\{f_\alpha(\mathbf{r}), f_\beta(\mathbf{r})\}$,

$$\rho_{\mu\nu} \approx \sum_\alpha c_{\nu\mu\alpha} f_\alpha + \sum_\beta c_{\mu\nu\beta} f_\beta \equiv \rho_{\mu\nu}^{\mathrm{PARI}} \tag{1}$$

where (in accordance with the convention introduced in section 1) the fit functions are defined to be centered on the second atom for each pair product. Similarly to the global "RI-V" approach[132,136] we define a residual vector

$$|\varepsilon_{\mu\nu}) = |\rho_{\mu\nu} - \rho_{\mu\nu}^{\mathrm{PARI}}) \tag{2}$$

and minimize the self-repulsion of the residual, $(\varepsilon_{\mu\nu}|\varepsilon_{\mu\nu})$. Essentially, this procedure minimizes the error in the electric field generated by the two charge distributions[191] and consequently minimizes the error in the representation of the ERIs.[136] It leads to a set of linear equations for the determination of the fit coefficients (where the inverse of the matrix V can always be calculated in a numerically stable way using a singular value decomposition (SVD)),

$$c_{\nu\mu\alpha} = \sum_\beta O_{\mu\nu\beta}[V^{-1}]_{\alpha\beta} \tag{3}$$

with the electrostatic interaction between the product of AOs and fit functions,

$$O_{\mu\nu\beta} = \int_{\mathbb{R}^3} \mathrm{d}\mathbf{r}\, \chi_\mu(\mathbf{r})\, \chi_\nu(\mathbf{r})\, v_\beta(\mathbf{r}) \tag{4}$$

and the electrostatic interaction (Coulomb overlap) between fit functions,

$$V_{\alpha\beta} = \int_{\mathbb{R}^3} \mathrm{d}\mathbf{r}\, v_\alpha(\mathbf{r})\, f_\beta(\mathbf{r}) \tag{5}$$

where the electrostatic potential v due to the function f_α has been introduced as

$$v_\alpha(\boldsymbol{r}) = \int_{\mathbb{R}^3} \mathrm{d}\mathbf{r}'\, f_\alpha(\mathbf{r}') \frac{1}{|\mathbf{r} - \mathbf{r}'|} \tag{6}$$

Using (1) and (5), the elements of the ERI tensor (in Mulliken notation) might be expressed as

$$\begin{aligned}(\mu\nu|\kappa\lambda) &= (\rho_{\mu\nu}|\rho_{\kappa\lambda}) \\ &\approx (\rho_{\mu\nu}^{\mathrm{PARI}}|\rho_{\kappa\lambda}^{\mathrm{PARI}}) \\ &= \sum_{\beta\delta} c_{\mu\nu\beta} V_{\beta\delta} c_{\kappa\lambda\delta} + \sum_{\alpha\delta} c_{\nu\mu\alpha} V_{\alpha\delta} c_{\kappa\lambda\delta} \\ &\quad + \sum_{\beta\gamma} c_{\mu\nu\beta} V_{\beta\gamma} c_{\lambda\kappa\gamma} + \sum_{\alpha\gamma} c_{\nu\mu\alpha} V_{\alpha\gamma} c_{\lambda\kappa\gamma}\end{aligned} \tag{7}$$

With the set of eqs 1−7, we have essentially expressed the fourth-order ERI tensor in terms of a set of third-order and second-order tensors of quadratically growing cardinality, where the number of elements of each tensor is small and independent of the system size. Compared to global DF, the complexity of computing the exact exchange regarding both CPU time and memory requirements is greatly reduced: First, the number of equations that have to be solved in the fitting procedure is equal to the number of negligible AO products,[183] which always scales linearly with system size. Second, the memory requirements are brought down to quadratic and further to linear when insignificant pair densities are not fitted. Finally, the exact exchange matrix is evaluated in N^3: With eq 7, the elements of the exchange matrix $K_{\tilde{\mu}\tilde{\kappa}}$ might be expressed as

$$K_{\tilde{\mu}\tilde{\kappa}} = K_{\mu\kappa} \qquad \forall\, A,\, C \in N_{\mathrm{a}} \tag{8}$$

$$\begin{aligned}K_{\mu\kappa} &\approx \sum_{\nu\lambda} P_{\nu\lambda} \sum_{\beta\delta} c_{\mu\nu\beta} V_{\beta\delta} c_{\kappa\lambda\delta} + \sum_{\nu\lambda} P_{\nu\lambda} \sum_{\alpha\delta} c_{\nu\mu\alpha} V_{\alpha\delta} c_{\kappa\lambda\delta} \\ &\quad + \sum_{\nu\lambda} P_{\nu\lambda} \sum_{\beta\gamma} c_{\mu\nu\beta} V_{\beta\gamma} c_{\lambda\kappa\gamma} + \sum_{\nu\lambda} P_{\nu\lambda} \sum_{\alpha\gamma} c_{\nu\mu\alpha} V_{\alpha\gamma} c_{\lambda\kappa\gamma} \\ &= K_{\mu\kappa}^{\mathrm{I}} + K_{\mu\kappa}^{\mathrm{II}} + (K^{\mathrm{II}})_{\mu\kappa}^{\mathrm{T}} + K_{\mu\kappa}^{\mathrm{III}}\end{aligned} \tag{9}$$

where $P_{\mu\nu}$ denotes elements of the density matrix. Cubic scaling is reached as it is possible to arrange all contractions in a way that never more than three atomic centers are involved. Taking into account distance effects, the scaling (with regard to both timing and memory) can be further brought down to linear as we will elaborate in section 2.5.

2.2. Numerical Considerations and Fit Set Quality. Compression of the ERI tensor via auxiliary basis set expansions usually introduces fitting errors ϵ in the ERIs (see (2)), where $\epsilon \to 0$ when the auxiliary basis approaches completeness. The rate of convergence of the auxiliary basis set expansion obviously depends strongly on the chosen fitting metric as well as on the nature of the fitting procedure: *Robust* fitting,[138]

$$(\rho_{\mu\nu}|\rho_{\kappa\lambda}) \approx (\rho_{\mu\nu}^{\mathrm{PARI}}|\rho_{\kappa\lambda}) + (\rho_{\mu\nu}|\rho_{\kappa\lambda}^{\mathrm{PARI}}) - (\rho_{\mu\nu}^{\mathrm{PARI}}|\rho_{\kappa\lambda}^{\mathrm{PARI}}) \tag{10}$$

shows an error ϵ falling off bilinearly with the fitting error. However, due to its much lower computational complexity, we rely on *nonrobust* fitting instead,

$$(\rho_{\mu\nu}|\rho_{\kappa\lambda}) \approx (\rho_{\mu\nu}^{\mathrm{PARI}}|\rho_{\kappa\lambda}^{\mathrm{PARI}}) \tag{11}$$

resulting in errors linear in the fitting error.[189] Consequently, due to the small number of auxiliary fit functions used to expand the pair densities (when compared to global fitting approaches), one would expect rather large errors in the computed integrals. However, the PARI-ERIs are usually very accurate approximations to the ERIs obtained without DF.[187] The exchange energy contribution (and consequently the HF/Hybrid-KS-DFT energy) from nonrobust fitting is unbounded from below,[183] making the SCF variationally unstable especially for large basis sets; calculations using quadruple-ζ-quality basis sets are often unreliable. The procedure becomes numerically more stable when rather large auxiliary fit sets are used.[186,189] In ADF, they are obtained as even-tempered series,[192−194] where the quality is controlled by the number of fit functions placed within a given range from the atomic

https://dx.doi.org/10.1021/acs.jctc.9b00854
J. Chem. Theory Comput. 2020, 16, 875−891

Table 1. Number of Auxiliary Fit Functions (Angular Part Expressed in Real Spherical Harmonics) for Representative Types of Atoms for Different Fit Set Qualities on the All-Electron Level

	no. of auxiliary functions (composition)		
quality	H	C	Au
Normal	62 (6s5p4d3f)	117 (10s9p5d4f3g)	779 (28s28p23d19f16g12h11i)
VeryGood	132 (10s7p6d5f4g)	209 (21s12p11d7f6g)	858 (31s22p20d19f16g16h16i)

center. Table 1 shows the number of fit functions for representative atom types for the fit sets employed in this work.

2.3. DF-MP2 and AO-MP2 Equations. The canonical MP2 correlation energy $E_{\mathrm{corr}}^{\mathrm{MP2}}$ for a closed shell molecule can be expressed as

$$E_{\mathrm{corr}}^{\mathrm{MP2}} = -\sum_{ij,ab}^{\mathrm{occ,virt}} \frac{(ia|jb)[2(ia|jb) - (ib|ja)]}{\epsilon_a + \epsilon_b - \epsilon_i - \epsilon_j} \tag{12}$$

where $(ia|jb)$ denotes an ERI in Mulliken notation, i, j (a, b) denote occupied (virtual) MO indices and ϵ_i (ϵ_a) denote diagonal elements of the occupied (virtual) blocks of the Fock matrix in the MO basis. Due to the transformation of the ERIs from the AO to the MO basis, the computational effort for the evaluation of this expression scales as N^5. Using global DF, the prefactor of the computation of $E_{\mathrm{corr}}^{\mathrm{MP2}}$ can be lowered considerably. The four-center integrals in the AO basis are then expressed as

$$(\tilde{\mu}\tilde{\nu}|\tilde{\kappa}\tilde{\lambda}) = \sum_{\tilde{\beta}\tilde{\delta}} C_{\tilde{\mu}\tilde{\nu}\tilde{\beta}} V_{\tilde{\beta}\tilde{\delta}} C_{\tilde{\kappa}\tilde{\lambda}\tilde{\delta}} \tag{13}$$

with the third-order tensor $C_{\tilde{\mu}\tilde{\nu}\tilde{\alpha}}$ and second-order tensor $V_{\tilde{\alpha}\tilde{\beta}}$. With any local fitting approach, the MP2 energy can be evaluated in exactly the same way. Within the PARI approach one might simply obtain $C_{\tilde{\mu}\tilde{\nu}\tilde{\alpha}}$ and $V_{\tilde{\alpha}\tilde{\beta}}$ from

$$\left.\begin{aligned} C_{\tilde{\mu}\tilde{\nu}\tilde{\beta}} &= C_{\tilde{\nu}\tilde{\mu}\tilde{a}} = (1 + \delta_{AB}) c_{\mu\nu\beta} \\ V_{\tilde{\beta}\tilde{\delta}} &= V_{\beta\delta} \end{aligned}\right\} \quad \forall\, B, D \in N_{\mathrm{a}} \tag{14}$$

In fact, employing PARI the prefactor of canonical DF-MP2 could be reduced further using sparse matrix algebra (the rank of the third-order tensor only scales linearly). In this work, we have not explored this possibility as far greater speed-up can be achieved working in the AO basis.

Applying the transformation

$$\begin{aligned} \frac{1}{\epsilon_a + \epsilon_b - \epsilon_i - \epsilon_j} &= \int_0^\infty \mathrm{d}t\ \mathrm{e}^{-(\epsilon_a+\epsilon_b-\epsilon_i-\epsilon_j)t} \\ &\approx \sum_{\tau}^{N_{\mathrm{q}}} \omega_\tau \mathrm{e}^{-(\epsilon_a+\epsilon_b-\epsilon_i-\epsilon_j)\tilde{\alpha}_\tau} \end{aligned} \tag{15}$$

suggested by Häser and Almlöf[150−152] results in

$$E_{\mathrm{corr}}^{\mathrm{MP2}} = -\sum_{\tau}^{N_{\mathrm{nq}}} \omega_\tau e_\tau^{(2)} = -\sum_{\tau}^{N_{\mathrm{nq}}} \omega_\tau (2e_J^{(2)^\tau} - e_K^{(2)^\tau}) \tag{16}$$

with

$$e_J^{(2)^\tau} = \sum_{\mu\nu\kappa\lambda} (\underline{\mu\bar{\nu}}|\underline{\kappa}\bar{\lambda})^{(\tau)} (\tilde{\nu}\tilde{\mu}|\tilde{\kappa}\tilde{\lambda}) \tag{17}$$

and

$$e_K^{(2)^\tau} = -\sum_{\mu\nu\kappa\lambda} (\underline{\mu\bar{\nu}}|\underline{\kappa}\bar{\lambda})^{(\tau)} (\tilde{\nu}\tilde{\mu}|\tilde{\kappa}\tilde{\lambda}) \tag{18}$$

The sum over τ and the weight ω_τ in (16)−(18) result from the evaluation of (15) by numerical quadrature. The optimal values for the set of quadrature points $\{\tilde{\alpha}_\tau\}_{\tau=1,\ldots,N_{\mathrm{q}}}$ and weights $\{\omega_\tau\}_{\tau=1,\ldots,N_{\mathrm{q}}}$ can simply be obtained by least-squares minimization of the error distribution function

$$\begin{aligned} \tilde{\eta}_k(x;\ \{\omega_\tau\},\ \{\tilde{\alpha}_\tau\}) &= \sum_{\tau}^{N_{\mathrm{q}}} \omega_\tau \mathrm{e}^{-x\tilde{\alpha}_\tau} - \frac{1}{x}, \\ x &= \epsilon_a + \epsilon_b - \epsilon_i - \epsilon_j \end{aligned} \tag{19}$$

however, the minimax approximation[195,196] is a computationally more efficient approach. $(\underline{\mu\bar{\nu}}|\underline{\kappa}\bar{\lambda})^{(\tau)}$ is obtained by transformation of the AO-ERI tensor according to

$$(\underline{\mu\bar{\nu}}|\underline{\kappa}\bar{\lambda})^{(\tau)} = \sum_{\tilde{\mu}'\tilde{\nu}'\tilde{\kappa}'\tilde{\lambda}'} P_{\tilde{\mu}\tilde{\mu}'}^{(\tau)} Q_{\tilde{\nu}\tilde{\nu}'}^{(\tau)} (\tilde{\mu}'\tilde{\nu}'|\tilde{\kappa}'\tilde{\lambda}') P_{\tilde{\kappa}\tilde{\kappa}'}^{(\tau)} Q_{\tilde{\lambda}\tilde{\lambda}'}^{(\tau)} \tag{20}$$

employing the PDMs $\mathbf{P}^{(\tau)}$ and $\mathbf{Q}^{(\tau)}$, given as

$$\begin{aligned} P_{\tilde{\mu}\tilde{\mu}'}^{(\tau)} &= \sum_{i}^{\mathrm{occ}} c_{\tilde{\mu}i} e^{\epsilon_i t_\tau} c_{i\tilde{\mu}'}, \\ Q_{\tilde{\nu}\tilde{\nu}'}^{(\tau)} &= \sum_{a}^{\mathrm{virt}} c_{\tilde{\nu}a} e^{-\epsilon_a t_\tau} c_{a\tilde{\mu}'} \end{aligned} \tag{21}$$

The quality of MP2 energies can generally be improved by empirically scaling individual contributions to it, giving rise to the popular spin-component-scaled (SCS)-[115,197−199] and spin-opposite-scaled-(SOS) MP2[116,117,200,201] approaches, where SCS-MP2 is often more accurate than SOS-MP2. However, for SOS-MP2 the second term on the right-hand side of (16) is completely neglected and the SOS-MP2 energy is obtained from

$$E_{\mathrm{corr}}^{\mathrm{SOS\text{-}MP2}} = -c_{\mathrm{SOS}} \sum_{\tau}^{N_{\mathrm{nq}}} \omega_\tau e_J^{(2)^\tau} \tag{22}$$

where usually $c_{\mathrm{SOS}} = 1.3$ is chosen.[116] This part of the MP2 energy can be evaluated with considerably lower computational cost than the same-spin part as it factorizes in a more favorable way and tensor contraction techniques can be used more efficiently.[164,180,181] Given the fact that DHs based on SOS-MP2 usually come very close to the accuracies of SCS-MP2 based ones,[127,202] the construction of fast SOS-MP2 methods alone seems to be highly desirable. Thus, in our efforts to develop a low-cost MP2 implementation, we have focused on the evaluation of $e_J^{(2)^\tau}$ only. The resulting algorithm and its implementation will be the subject of the next sections.

2.4. SOS-AO-PARI-MP2 Equations. In the AO basis, $E_{\mathrm{corr}}^{\mathrm{MP2}}$ can be obtained from summing up the contributions from all pairs of atoms. Such a decomposition has already been suggested by Ayala and Scuseria nearly two decades ago;[203]

https://dx.doi.org/10.1021/acs.jctc.9b00854
J. Chem. Theory Comput. 2020, 16, 875−891

here it arises quite naturally from the PARI approach. In particular, the Coulomb term can be obtained from

$$e_J^{(2)} = \sum_{AB} e_J^{(2)^{AB}}, \qquad e_J^{(2)^{AB}} = e_J^{(2)^{BA}}$$

where $e_J^{(2)^{AB}}$ denotes the contribution to $e_J^{(2)}$ from atom pair (A, B). Inserting (7) into (17) and dropping the index τ in the following, we obtain with the help of (20)

$$\begin{aligned} e_J^{(2)^{AB}} = \sum_{\mu\nu\kappa\lambda\mu'\nu'\kappa'\lambda'} P_{\mu\mu'}P_{\kappa\kappa'}Q_{\nu\nu'}Q_{\lambda\lambda'} \times \Bigg\{ \sum_{\beta\delta} c_{\mu\nu\beta}V_{\beta\delta}c_{\kappa\lambda\delta} \\ + \sum_{\alpha\delta} c_{\nu\mu\alpha}V_{\alpha\delta}c_{\kappa\lambda\delta} + \sum_{\beta\gamma} c_{\mu\nu\beta}V_{\beta\gamma}c_{\lambda\kappa\gamma} + \sum_{\alpha\gamma} c_{\nu\mu\alpha}V_{\alpha\gamma}c_{\lambda\kappa\gamma} \Bigg\} \\ \times \Bigg\{ \sum_{\beta'\delta'} c_{\mu'\nu'\beta'}V_{\beta'\delta'}c_{\kappa'\lambda'\delta'} + \sum_{\alpha'\delta'} c_{\nu'\mu'\alpha'}V_{\alpha'\delta'}c_{\kappa'\lambda'\delta'} + \\ \sum_{\beta'\gamma'} c_{\mu'\nu'\beta'}V_{\beta'\gamma'}c_{\lambda'\kappa'\gamma'} + \sum_{\alpha'\gamma'} c_{\nu'\mu'\alpha'}V_{\alpha'\gamma'}c_{\lambda'\kappa'\gamma'} \Bigg\} \end{aligned} \tag{23}$$

Equation 23 factorizes (unlike the corresponding expressions for $e_K^{(2)^{AB}}$) according to

$$e_J^{(2)^{AB}} = \sum_{\alpha\beta} \left(\sum_{\alpha'} q_{\alpha\alpha'}V_{\alpha'\beta} \right) \left(\sum_{\beta'} V_{\alpha\beta'}q_{\beta'\beta} \right)^T \tag{24}$$

and $q_{\alpha\alpha'}$ (with $\mathbf{q}$ we will denote the set of all tensors $q^{AA'}$) is given as

$$\begin{aligned} q_{\alpha\alpha'} = \sum_{\mu\nu\mu'\nu'} [P_{\nu\nu'}Q_{\mu\mu'}c_{\nu\mu\alpha} + P_{\mu\mu'}Q_{\nu\nu'}c_{\nu\mu\alpha}]c_{\nu'\mu'\alpha'} \\ + \sum_{\mu\nu\mu'\nu'} [P_{\mu\nu}Q_{\mu'\nu'}c_{\nu'\mu\alpha} + P_{\mu'\nu'}Q_{\mu\nu}c_{\nu'\mu\alpha}]c_{\nu\mu'\alpha'} \end{aligned} \tag{25}$$

Equation 24 can be computed in N^3, and the same is true for (25): We first evaluate the local PDMs (21) for each pair of atoms. Then we half-transform the fit coefficients according to

$$\begin{aligned} e_{\nu'\mu\alpha} &= \sum_{\nu} P_{\nu'\nu}c_{\nu\mu\alpha}, \\ f_{\nu'\mu\alpha} &= \sum_{\nu} Q_{\nu'\nu}c_{\nu\mu\alpha} \end{aligned} \tag{26}$$

Both transformations only involve three atomic centers, namely, A, B, and B′. Furthermore, f and g are two-center quantities and the memory required to store $\mathbf{f}$ and $\mathbf{g}$ (the set of all tensors f/g for all pairs of atoms (A, A′)) scales quadratically with the number of atoms. Subsequently, the first term in (25) is evaluated according to

$$\begin{aligned} m_{\alpha\alpha'} &= \sum_{\mu\mu'\nu'} e_{\nu'\mu\alpha}Q_{\mu\mu'}c_{\nu'\mu'\alpha'} = \sum_{\mu'\nu'} \tilde{e}_{\nu'\mu'\alpha}c_{\nu'\mu'\alpha'}, \\ n_{\alpha\alpha'} &= \sum_{\mu\mu'\nu'} f_{\nu'\mu\alpha}P_{\mu\mu'}c_{\nu'\mu'\alpha'} = \sum_{\mu'\nu'} \tilde{f}_{\nu'\mu'\alpha}\, c_{\nu'\mu'\alpha'} \end{aligned} \tag{27}$$

and the second term as

$$\begin{aligned} g_{\alpha\alpha'} &= \sum_{\mu\mu'} e_{\mu'\mu\alpha}f_{\mu\mu'\alpha'}, \\ h_{\alpha'\alpha} &= \sum_{\mu\mu'} f_{\mu\mu'\alpha'}e_{\mu'\mu\alpha} \end{aligned} \tag{28}$$

resulting in

$$q_{\alpha\alpha'} = m_{\alpha\alpha'} + n_{\alpha\alpha'} + g_{\alpha\alpha'} + (h)^T_{\alpha\alpha'} \tag{29}$$

In fact, the chosen sequence of tensor contractions is closely related to a recent SOS-MP2 implementation by the Ochsenfeld group,[164] being even more apparent if one considers a monatomic system only for which the local pair fitting approach is equivalent to global DF. In all contraction steps, at most three atomic centers are involved, implying cubically scaling computation of the SOS-AO-MP2-PARI energy without any further consideration of distance effects. Furthermore, the three-center quantities $\tilde{f}$ and $\tilde{e}$ are evaluated on the fly, so that the memory requirements of the algorithm scale quadratically. As will be discussed in the next section, taking into account distance effects scaling of computation time and memory can be reduced further. We note that PARI also allows for quartic scaling computation of the exchange-like term in E_{corr}^{MP2}. At this point we want to emphasize the strong similarity of our algorithm to the THC-approach by Martinez and co-workers:[174,175,180,204] Both methods exploit the locality in the atomic orbital basis set directly by decomposition of the ERI tensor into factor matrices that grow initially as N^2, and as N as soon as a given system size is reached. Consequently, for the computation of E_{corr}^{MP2}, the same formal scaling is reached: N^3 for $e_J^{(2)}$ and N^4 for $e_K^{(2)}$.

2.5. Distance Effects. As the basis functions χ_μ, χ_ν are localized around their atomic centers, their overlap will decrease with increasing distance between the atoms on which they are centered. Consequently, the value of the overlap integral $O_{\mu\nu\beta}$ (eq 4) will approach zero with growing distance between the centers A and B. To exploit this behavior, we define a threshold $\vartheta_{DCAB} \in \mathbb{R}^+$ (we will refer to this approximation as *distant centers approximation for basis functions* (DCAB) in the following) and consider a basis function as negligible for $|\mathbf{r}| > d_\mu$ if

$$|\chi_\mu(\mathbf{r})| < \vartheta_{DCAB} \qquad \forall\ |\mathbf{r}| > d_\mu \tag{30}$$

where d_μ is some basis function dependent effective radius to be determined at runtime. The procedure is illustrated in Figure 1.

Consequently, we only compute the fit coefficient $c_{\nu\mu a}$ when

$$|\mathbf{R}_A - \mathbf{R}_B| < d_\mu + d_\nu \tag{31}$$

In practice, we reorder the basis functions from the most diffuse (most slowly decaying) to the tightest one for each atom A, so that the dimension of the fit function tensor c^{AB} approaches 0 for

$$|\mathbf{R}_A - \mathbf{R}_B| \to \infty \tag{32}$$

If

$$|\mathbf{R}_A - \mathbf{R}_B| > d_\mu + d_\nu \qquad \forall\ \mu, \nu \tag{33}$$

all tensor contractions involving the fit coefficient tensor corresponding to the pair (A, B) will be skipped. In the same way, we are also skipping tensor contractions involving the tensor V^{AB} if the range of the Coulomb potential due to A does

https://dx.doi.org/10.1021/acs.jctc.9b00854
J. Chem. Theory Comput. 2020, 16, 875−891

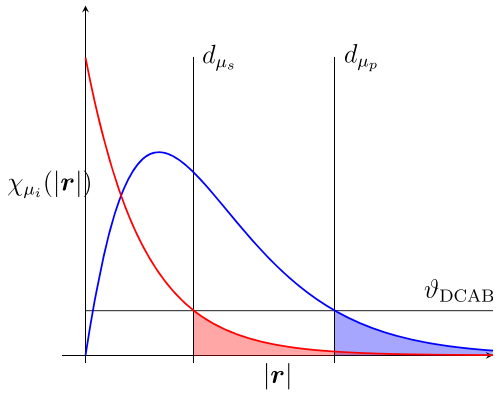

Figure 1. Schematic illustration of the dependence of d_μ on $\vartheta_{\mathrm{DCAB}}$ for two different types of functions. As a p-type function (blue) generally decays slower then an s-type one (red), its effective radius is larger.

not overlap with any basis function on B (*distant centers approximation for Coulomb potential* (DCAC)). As the Coulomb potential decays only as $|\mathbf{r}|^{-1}$, this approach will only be effective for very large molecules. However, the Coulomb potential due to a pair density can be approximated using the well-known multipole expansion of the Coulomb operator.[205] Thus, the interaction between two pair densities $\rho_{\mu\nu}$, $\rho_{\kappa\lambda}$ is evaluated via multipole expansion (recall that the fit functions are always assumed to be centered on the second atom of the pair) if

$$|\mathbf{R}_{\mathrm{B}} - \mathbf{R}_{\mathrm{D}}| > d_\beta + d_\delta \qquad \forall\, \beta, \delta \tag{34}$$

Similarly to the procedure for the basis functions, the actual values d_α are controlled via a threshold $\vartheta_{\mathrm{MA}} \in \mathbb{R}$. Considering multipole moments of up to $l_{\max} = 3$, the dimension of the tensor V^{BD} reduces to 16×16, for realistic fit sets being considerably lower than $N_{\mathrm{f}}^{\mathrm{A}} \times N_{\mathrm{f}}^{\mathrm{B}}$ (compare with Table 1). The multipole approximation (MA) as well as the DCAB and DCAF approximation are used to speed up the computation of the post-SCF energy correction and the SCF itself. Exclusively for the MP2 part, we exploit sparsity of the density matrix in a way that we avoid contractions with half-transformed fit function tensors if

$$\max_{\nu\mu\alpha} |x_{\nu\mu\alpha}| \leq \vartheta_{\mathrm{NHF}} \qquad \forall\, x_{\nu\mu\alpha} \in x,\ \vartheta_{\mathrm{NHF}} \in \mathbb{R}^+,\ x = f, g \tag{35}$$

We will refer to this approximation as *neglect of half-transformed fit coefficient tensors* (NHF) approximation. Clearly, as we do not use any localization techniques for the density matrix in our current implementation, this approximation can only be effective for spatially very extended systems. However, the density matrix and the half-transformed fit coefficient tensors show a high degree of sparsity, so that sparse matrix algebra techniques could efficiently be exploited here without a conceptual change of our implementation.

In practice, the efficiency of the possible screening options depends on thresholds, molecular geometry, and the diffuseness of the AO basis. Due to the rather large prefactor of $N_{\mathrm{f}}^2 N_{\mathrm{b}}^2$, the scaling is dominated by steps 3a/3b, whereas the computational time for step 1 is always negligible. The asymptotic scaling of wall clock time and memory of our algorithm under consideration of screening effects is presented in Table 2.

A very important question regarding the feasibility of a local MP2 computation is its memory requirement. The half-transformed fit coefficient tensors **f** and **g** can be kept in memory for rather large molecules consisting of several hundreds of atoms. Although the memory requirements for these quantities is formally linearly scaling, they can hamper the application of our algorithm to very large systems. However, storage of f and g for each pair of atoms can be avoided if these quantities are recalculated prior to the contraction (28) (i.e., if step 2a/2b is repeated before 4a/4b) and with slight changes of the loop structure, storage of **q** can also be avoided. As the number of non-negligible fit coefficients and fit functions grows linearly, our algorithm is then order-N in memory. We also note that the practical memory bottleneck in our implementation is the storage of the untransformed fit coefficient tensors for compact systems. This can be attributed to our large auxiliary fit sets and we are planning further optimizations in this direction.

2.6. Loop Structure and Parallelization. Our algorithm is implemented by setting up two nested loops running over all pairs of atoms, which are closed whenever a quantity needs to be stored for each pair. Whenever we sum over a third center, a third loop over atomic shells is invoked. To be memory efficient, the loops need to be organized in a way that storage of three-index quantities is always avoided. The concept is demonstrated for the K^{III} contribution to the exact exchange matrix in Algorithm 1 (see eq 9).

Table 2. Outline of the Basic SOS-AO-PARI-MP2 Contraction Steps with Asymptotic Scaling (Big-O Notation Implied) and Memory Requirements under Consideration of Distanc Effects[a]

step		asymptotic scaling	distance effects	memory
	calculate **P** and **Q**	N^3		$N_{\mathrm{b,all}}^2$
2a	$e_{\nu'\mu\alpha} = P_{\nu'\nu} c_{\nu\mu\alpha}$			
2b	$f_{\nu'\mu\alpha} = Q_{\nu'\nu} c_{\nu\mu\alpha}$	N^2	DCAB	$N_{\mathrm{a}}^2 N_{\mathrm{b}}^2 N_{\mathrm{f}}$ ($N_{\mathrm{a}} N_{\mathrm{b}}^2 N_{\mathrm{f}}$)
3a	$m_{\alpha\alpha'} = e_{\nu'\mu\alpha} Q_{\mu\mu'} c_{\nu'\mu'\alpha'}$			
3b	$n_{\alpha\alpha'} = f_{\nu'\mu\alpha} P_{\mu\mu'} c_{\nu'\mu'\alpha'}$	N	DCAB, NHF	on the fly
4a	$g_{\alpha\alpha'} = e_{\mu'\mu\alpha} f_{\mu\mu'\alpha'}$			
4b	$h_{\alpha'\alpha} = f_{\mu\mu'\alpha'} e_{\mu'\mu\alpha}$	N^2		on the fly
5	$q_{\alpha\alpha'} = m_{\alpha\alpha'} + n_{\alpha\alpha'} + g_{\alpha\alpha'} + (h)^{\mathrm{T}}_{\alpha\alpha'}$			$N_{\mathrm{a}}^2 N_{\mathrm{f}}^2$ ($N_{\mathrm{a}} N_{\mathrm{f}}^2$)
6	$Z_{\alpha\beta'} = q_{\alpha\alpha'} V_{\alpha'\beta'}$	N^2	MA, DCAF	
7	$e^{(2)^{\mathrm{AA}'}} = Z_{\alpha\alpha'} (Z^{\mathrm{T}})_{\alpha'\alpha}$	N^2		

[a]For each step the employed distance effects are given. The Einstein sum convention is used, which here always involves summation over the respective atomic centers. The memory requirements given in brackets refer to the memory saving variant of our algorithm.

https://dx.doi.org/10.1021/acs.jctc.9b00854
J. Chem. Theory Comput. 2020, 16, 875−891

Algorithm 1 Loop structure for the evaluation of the K^{III}-part of the exact exchange matrix including distance effects. Indices θ, ι refer to the MA.

```
K^III_μκ = 0
for A ∈ all, D ∈ all do
  for B ∈ all do
    if overlap negligible ∀(ν, μ) then
      skip pair (A,B)
    else
      (PC)_λμα += Σ_ν P_λν c_νμα ,   ν, μ non-negligible
      (PC)_λμθ += Σ_ν P_λν c_νμθ ,   ν, μ non-negligible
    end if
  end for
  for C ∈ all do
    if overlap negligible ∀(λ, κ) or (A, C) not Coulomb interacting then
      skip pair (A,C)
    end if
    if MA then
      (CV)_λκθ = Σ_ι c_λκι V_ιθ
    else
      (CV)_λκα = Σ_β c_λκβ V_βα
    end if
    K^III_μκ += Σ_λΩ (PC)_λμΩ (CV)_λκΩ ,   Ω = α or θ
  end for
end for
```

One might easily identify the first step in this algorithm as quadratically scaling, whereas the second one scales linearly. Although contractions involving V can rarely be skipped in practice, the multipole approximation considerably reduces the prefactor of this step. As the number of fit functions is usually larger than the number of basis functions, the second step determines the overall timing for the evaluation of K^{III}, explaining why we observe a subquadratic scaling behavior in practice (see section 3.3). The SOS-MP2 correlation energy can be evaluated in a similar way. The algorithm for steps 2a/2b is outlined in Algorithm 2. The aforementioned quadratic asymptotic scaling of this step can be verified easily.

Algorithm 2
Schematic implementation of step 2a/b from table 2.

```
for B' ∈ all, A ∈ all do
  e_ν'μα = 0
  f_ν'μα = 0
  for B ∈ all do
    if overlap negligible ∀(μ, ν) then
      skip pair (A,B)
    else
      e_ν'μα += Σ_ν P_ν'ν c_νμα   ν, μ ∈ non-negligible
      f_ν'μα += Σ_ν Q_ν'ν c_νμα   ν, μ ∈ non-negligible
    end if
  end for
  Save e_ν'μα, f_ν'μα for pair B', A
end for
```

The loop structure of the presented algorithms suggests a parallelization strategy in which the tensor contractions associated with a certain pair of atoms (A, D) are distributed over all processes. Each tensor contraction is then performed on a single core. To avoid overhead for the MP2 part, we employ a two-level parallelization strategy where all numerical quadrature points are distributed over all available nodes and second the outermost two nested loops over atomic shells are distributed over all cores on this node. Thus, the number of nodes that can be used efficiently is limited by the number of numerical quadrature points N_{nq} (usually less than 10). However, we do not expect this to be a relevant issue for the most probable targets of our algorithm.

3. BENCHMARK CALCULATIONS AND DISCUSSION

3.1. Computational Details. We performed PARI-MP2 and SOS-AO-PARI-MP2 calculations with a locally modified development version of ADF.[137,206,207] We employed standard STO basis sets[190] and auxiliary fit sets for the evaluation of the exact exchange as described in section 2.2. If not indicated otherwise, all computations have been performed on the all-electron level.

To rule out the possibility of numerical issues throughout our benchmark calculations, the numerical integration quality, as well as the quality of the DF for the Coulomb part,[208] has been chosen to be better than default (*Good* quality, see refs 208 and 209) if not stated otherwise. For the SCF, the mixed ADIIS+SDIIS method[210] has been employed.

All dimerization energies have been computed using the counterpoise (CP) method of Boys and Bernardi[211] to correct the basis set superposition error (BSSE). For all systems involving transition metals, relativistic effects have been treated with the zero-order regular approximation (ZORA)[212−215] in conjunction with ZORA-optimized basis sets and the minimum of neutral atomic potential approximation (MAPA).

If not stated otherwise, we used $N_{nq} = 6$ for all SOS-AO-PARI-MP2 calculations, where the numerical quadrature has been performed with a code[216] developed by Helmich-Paris.[195,196] For the evaluation of the exact exchange as well as for all SOS-AO-PARI-MP2 calculations, the default screening thresholds are

$$\vartheta_{NHF} = 1 \times 10^{-10},$$
$$\vartheta_{MA} = 3 \times 10^{-2},$$
$$\vartheta_{DCAF} = 1 \times 10^{-3},$$
$$\vartheta_{DCAB} = 1 \times 10^{-3} \quad (36)$$

All calculations presented in this work were performed on a 2.2 GHz intel Xeon (E5-2650 v4) with 24 cores and 128 GB RAM. All binaries have been created using the GNU Fortran compiler.

3.2. Accuracy and Convergence with Basis Set Size. In this section we want to assess (a) the error introduced by the PARI-approach compared to that introduced by canonical DF-MP2, (b) the numbers of auxiliary fit functions required for accurate results as well as for a numerically stable SCF, and (c) the quality of our standard, non-correlation consistent STO basis sets. To this end, we performed benchmark calculations on different popular test sets: These are the s66 test set of weak intermolecular interactions[217] and test sets of relative conformational energies from the GMTKN30 database.[218] To assess the accuracy of our implementation in conjunction with an approximate treatment of relativistic effects, we calculated the HEAVY28 test sets of noncovalent interactions between heavy element hydrides.[219] We also report results for the L7[220] test set of weak intermolecular interactions with dimers of between roughly 50−120 atoms to asses the performance of our SOS-AO-PARI-MP2 implementation for large molecules. The entirety of all these test sets comprises of 187 data points.

We calculated the s66 test set of weak intermolecular interactions (London dispersion, hydrogen binding, $\pi-\pi$ interactions) using TZP (triple-ζ with single shell of polarization functions) and TZ2P (triple-ζ with two shells of polarization functions) basis sets in conjunction with the *Normal* auxiliary fit set (see Table 1 for the number of auxiliary fit functions for selected atoms). Figure 2 shows deviations from our results to DF-MP2/CBS reference values[217] for all individual data points as well as mean absolute deviations (MAD) for each basis set. It is well-known that extrapolation to the basis set limit is only possible when correlation consistent basis sets of systematically increasing size are employed.[29] As a consequence, comparison of PARI-MP2/

https://dx.doi.org/10.1021/acs.jctc.9b00854
J. Chem. Theory Comput. 2020, 16, 875−891

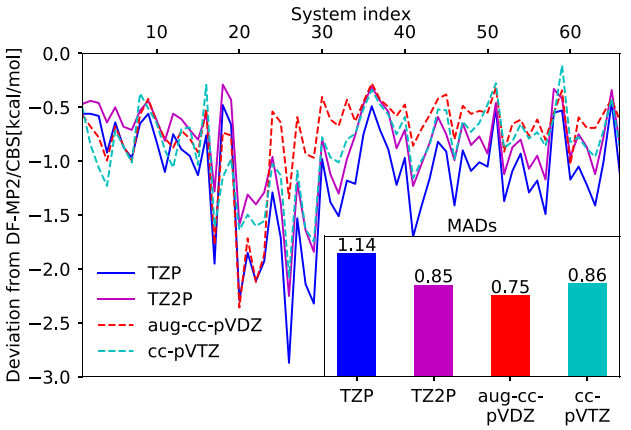

Figure 2. Deviations from basis set extrapolated DF-MP2/CBS reference values[217] (in kcal/mol) for different basis sets for each data point in the s66[217] test set of weak intermolecular interactions. The aug-cc-pVDZ and cc-pVTZ reference values[217] have been computed with DF-MP2, whereas the TZP and TZ2P values have been obtained with our PARI-MP2 code, using the *Normal* fit set for both HF and MP2. MADs are given with respect to DF-MP2/CBS.

TZP(TZ2P) calculations to DF-MP2/CBS results cannot reveal if deviations can be attributed to basis set incompleteness or to the local pair fitting approach. To obtain a clearer idea about the reasons for the observed deviations from the DF-MP2/CBS results, we also compare our computed energies to DF-MP2/aug-cc-pVDZ and DF-MP2/cc-pVTZ reference values.[217] Both basis sets are comparable in size with TZP and TZ2P, with cc-pVTZ being the largest basis set with three shells of polarization functions, and TZP the smallest one, and the only one with only one shell of polarization functions. Figure 2 clearly demonstrates that calculations on PARI-MP2/TZ2P/*Normal*-level yield results comparable to those of DF-MP2/aug-cc-pVDZ and DF-MP2/cc-pVTZ, with a MAD slightly better than DF-MP2/cc-pVTZ and slightly worse than DF-MP2/aug-cc-pVDZ. Also the sign-corrected maximum errors are with 2.8 kcal/mol for TZP and 2.3 kcal/mol for TZ2P in line with the two Gaussian type orbital (GTO) basis sets for which Figure 2 also shows maximum errors considerably larger than 2 kcal/mol. Although the computed energies are on average very close to reproducing the DF-MP2/CBS references within a chemical accuracy of 1 kcal/mol, the PARI-MP2/TZP results are generally inferior to their TZ2P counterparts, which can safely be attributed to the smaller number of polarization functions.

From the good agreement of our PARI-MP2 results with DF-MP2 for basis sets of comparable size, we conclude that the PARI-approximation does not seem to considerably degrade the accuracy of DF-MP2 dimerization energies. Furthermore, our findings suggest that our non-correlation consistent STO-type basis sets can compete with larger correlation consistent GTO-type basis sets with more shells of polarization functions.

A factor, not having been discussed so far, is the size of the auxiliary fit sets. As already pointed out, a lager fit set should help to ensure variational stability of the HF energy in the SCF. To this end, we computed the relative conformational energies in the GNTKM30 database (the ACONF, SCONF, PCONF, CyCONF, and ISO34 subsets) with *Normal* and *VeryGood* fit set for both HF and PARI-MP2 and also recalculated the s66 dimerization energies with the larger auxiliary fit set. Somewhat surprisingly, we found that the larger auxiliary fit set sometimes led to deteriorated PARI-MP2 energies, especially for the S66 test set, whereas the HF energies remained essentially unchanged (as expected). This observation is directly opposed to the fact that larger fit sets should generally improve any DF approximation.

We then carried out calculations where we retained the *VeryGood* fit set for the SCF but used the *Normal* fit set for the evaluation of the MP2 energy correction; i.e., we recalculated the ERIs after convergence of the SCF using a smaller fit set. The results are summarized in Figure 3.

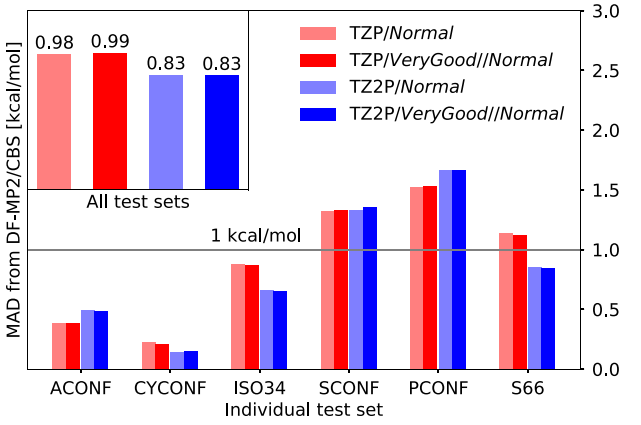

Figure 3. PARI-MP2 results (in kcal/mol) for selected test sets of isomerization energies from the GNTKM30 benchmark set[218] as well as for the s66 test set. The MADs for each data set with respect to DF-MP2/CBS, as well as the MADs for the entirety of all test sets (in total 152 data points) are given. Key: basis set/HF auxiliary fit set//MP2 auxiliary fit set.

Clearly, for almost all test sets, the computed energies are nearly independent of the auxiliary fit set employed in the SCF. This is reflected in the MADs over all test sets, where literally no difference can be observed between *Normal* and *VeryGood*. Only for the SCONF test set, the *VeryGood* fit set is slightly inferior to *Normal*.

As recalculation of the ERIs after the SCF seems to cure the problems in the computation of the PARI-MP2 energy for the *VeryGood* fit set, one must conclude that neither the MOs nor the orbital energies resulting from the use of this fit set are problematic for the computation of $E_{\mathrm{corr}}^{\mathrm{MP2}}$, but rather the fitting errors in the ERIs themselves. Due to the fact that for some test sets the *VeryGood* fit set yielded (rather small) improvements over the *Normal* one, we do not suspect a fundamental issue with the PARI approximation here but rather a numerical one. Clearly, the large number of auxiliary fit functions for the expansion of each pair of basis functions leads to linear dependencies in the fit set that might cause numerical problems due to overfitting. We emphasize that the *VeryGood* fit set is usually not inferior to the *Normal* one. However, the latter one seems to be numerically more stable for PARI-MP2 calculations and also completely sufficient for the purpose of the present study. Optimizing fit sets specifically for correlation methods seems to be highly promising for even more accurate PARI-MP2 energies but is out of the scope of this work.

The clearly improved results over the TZP basis set when TZ2P is used for the s66 test set can generally not be observed for the test sets of conformers. For the ACONF (alkane conformers) and PCONF (tripeptide conformers) test sets, the

https://dx.doi.org/10.1021/acs.jctc.9b00854
J. Chem. Theory Comput. 2020, 16, 875−891

Table 3. Maximum Sign Corrected Errors for the S66 Test Set and the Test Sets of Relative Conformational Energies for the Herein Investigated Combinations of Basis Sets and Fit Sets (All Energies in kcal/mol)[a]

test set/fit set	ACONF	CYCONF	ISO34	SCONF	PCONF	S66
TZP/*VeryGood*//*Normal*	0.68	0.50	3.86	3.20	3.46	2.83
TZ2P/*VeryGood*//*Normal*	0.93	0.28	3.62	3.09	3.79	2.13
TZP/*Normal*	0.67	0.53	3.87	3.20	3.45	2.87
TZ2P/*Normal*	0.92	0.25	3.56	3.08	3.76	2.25

[a]First column: basis set/HF auxiliary fit set (//MP2 auxiliary fit set).

TZP energies are even slightly better than the TZ2P ones. This can only be explained with error cancellation: It is well-known that MP2 often tends to overestimate correlation energies,[221] so that a more incomplete basis set might yield better results for certain systems. Only for CYCONF (cysteine conformers) and ISO34 (isomerization energies of organic molecules), a clear improvement over TZP can be observed when TZ2P is used instead. As the overall MADs over all 152 data points reveal, all considered combinations of basis and fit sets reproduce the DF-MP2/CBS reference within chemical accuracy on average, where the TZ2P basis set is in many (but not all) cases superior to TZP.

As shown in Table 3, we find only moderate maximum errors for the CYCONF and ACONF test sets with 0.5 and 0.7 kcal/mol, respectively for the TZP basis set and 0.3 and 0.9 kcal/mol, respectively, for the TZ2P one. For the SCONF and PCONF test sets we find larger maximum errors of over three kcal/mol irrespective of basis set and fit set and nearly 4 kcal/mol for the ISO34 test set with the TZP basis set, reflecting the slow basis set convergence of MP2 correlation energies.

As our findings show that the more expensive *VeryGood* fit set yields no improvement over the *Normal* one, we strongly recommend using the latter one. Considering error cancellation between $e_J^{(2)}$ and $e_K^{(2)}$ as highly unlikely, our findings also apply to all spin-scaled variants of MP2.

For heavy elements we found excellent agreements to the CCSD(T)/CBS reference values for the HEAVY28 test set.[219] Already on the TZP/*Normal*/ZORA-level, our results show a MAD of only 0.30 kcal/mol. This is actually better than DF-MP2/CBS for which a MAD of 0.41 kcal/mol has been reported when small effective core potentials of the Stuttgart/Cologne group[222,223] for elements with $Z > 36$ are used.

After having assessed the performance of our MO based PARI-MP2 algorithm, we finally explore the accuracy of our SOS-AO-PARI-MP2 implementation for large molecules. To this end, we computed the dimerization energies from the L7 test set with varying thresholds controlling the distance effects outlined in section 2.5. As we are not aware of SOS-MP2 reference energies for this test set, we compare our results to the available QCISD(T)/CBS values.[217] We emphasize that the only approximation in SOS-AO-PARI-MP2 that is not already present in SOS-PARI-MP2 is the numerical quadrature (15). For an account on its convergence with respect to N_{nq} we refer to the literature.[164] We only note that $N_{nq} = 6$ is usually sufficient to achieve millihartree accuracy. However, a broader range of orbital energies and a smaller HOMO−LUMO gap require more quadrature points and $N_{nq} = 8$ might be more appropriate. To rule out the possibility of inaccuracies due to a too small N_{nq}, we have decided to use $N_{nq} = 8$ for the numerical computation of (15).

First, we tested the performance of our method for different thresholds, controlling the distance effects described in section 2.5. We do not consider variations of ϑ_{NHF} here and also found it useful to group the remaining thresholds in tiers. For each of these tiers, as described in Table 4, we have calculated the L7 test set with the TZP basis set and the *Normal* auxiliary fit set. Our results are shown in Figure 4, where the upper part shows the deviations of computed reaction energies with respect to the *Basic* tier. Going up to the *Normal* tier (painted area), the largest change in energies occurs for c3gc with roughly 0.3 kcal/mol. Proceeding from *Normal* to *Good*, the energy does only change marginally for all dimers, justifying the *Normal* tier as our default. Essentially no difference can be observed between the last two tiers.

Table 4. Definition of Threshold Tiers

	Basic	*Normal*	*Good*	*VeryGood*
ϑ_{DCAB}	2×10^{-3}	1×10^{-3}	3×10^{-4}	1×10^{-4}
ϑ_{DCAC}	2×10^{-2}	1×10^{-2}	1×10^{-3}	1×10^{-4}
ϑ_{MA}	3×10^{-2}	3×10^{-3}	3×10^{-3}	3×10^{-4}

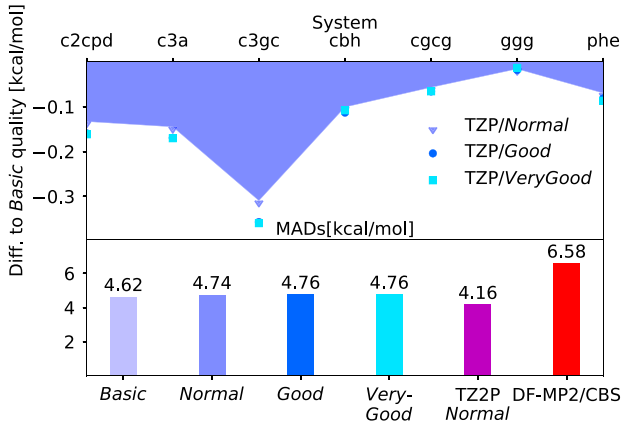

Figure 4. Upper part: Deviations from results obtained with the *Basic* tier of thresholds for the individual reaction energies. Lower panel: MADs with respect to the QCISD/CBS reference[217] for SOS-AO-PARI-MP2 calculations, as well as for DF-MP2/CBS. All energies are in kcal/mol. The naming of the dimers follows Řezáč et al.[217]

As shown in the lower half of Figure 4, using smaller thresholds leads to an artificial improvement of the dimerization energies: MP2 often exaggerates correlation effects as its double excitations do not couple.[221] Lowering the cutoff thresholds, however, corresponds to the neglect of correlation from distant pairs. Thus, the underestimation of dispersion interactions due to the neglect of long-range correlation effects partly compensates for the overestimation of the correlation energy within MP2, explaining the trend in the observed reaction energies.

We finally note that the TZ2P basis set gives improvements over TZP, although the MAD is still higher than 4 kcal/mol.

https://dx.doi.org/10.1021/acs.jctc.9b00854
J. Chem. Theory Comput. 2020, 16, 875−891

However, this is significantly better than full DF-MP2/CBS calculations for which a MAD of 6.58 kcal/mol has been reported in the literature.[217]

To conclude this section, we think that the presented data clearly demonstrates (i) that our default fit set is completely sufficient to compute accurate PARI-MP2 energies in a numerically stable way, (ii) that the deviation from the DF-MP2/CBS reference values can (at least to a great extent) be attributed to the basis set error, (iii) that our PARI-MP2 implementation used with non-correlation consistent basis sets of triple-ζ quality yields errors comparable to the ones from DF-MP2 with correlation consistent basis sets of the same size, and finally, (iv) that our implementation also yields accurate and reliable energies for large systems when rather conservative default screening thresholds are used.

3.3. Performance and Timing. We analyzed the performance of our SOS-AO-PARI-MP2 implementation on a series of linear alkane chains as an optimum-case for local correlation methods. Our results are summarized in Table 5.

Table 5. CPU Times and Scaling Behavior with Respect to the Systems Size Relative to the Previous Calculation (in Parentheses) in Terms of the Polynomial Coefficient x in N^x for SOS-AO-PARI-MP2 Calculations on Linear Alkane Systems Using TZP and TZ2P, Respectively, and *Normal* Fit Set Quality (All Calculations on a Single Core, All Timings in min)

		timing				
n (C_nH_{2n+2})	no. of bf	total		MP2 alone		MP2 time [% of full calc]
		TZP				
20	632	23.5		3.9		16.6
40	1252	76.8	(1.70)	17.5	(2.16)	22.8
80	2492	255.3	(1.79)	75.3	(2.11)	29.5
160	4972	907.3	(1.83)	323.6	(2.10)	35.6
		TZ2P				
20	1084	41.7		8.4		20.1
40	2144	139.4	(1.74)	37.4	(2.15)	26.8
80	4264	473.0	(1.76)	156.0	(2.06)	33.0
160[a]	8504	1811.2	(1.94)	752.3	(2.27)	41.5

[a]Calculated with the more memory efficient variant of the algorithm.

In all computations, the evaluation of the MP2 correlation energy only accounts for between 20 and 42% of the total wall clock time. Thus, the overall scaling is dominated by the HF part, reaching subquadratic scaling already for the shortest chains considered here, whereas for the computation of the post-SCF energy correction quadratic scaling is observed for both basis sets. This can be attributed to the rather conservatively chosen screening thresholds due to which NHF screening becomes practically irrelevant, even for large and spatially extended systems. It should also be emphasized that the scaling is not strongly affected by the number of diffuse functions in the basis set. For the TZ2P basis set containing a larger number of diffuse polarization functions, the scaling is even slightly better than for the TZP basis set. Due to the huge memory requirements to store **f** and **g**, we have been forced to switch to the slightly slower, but more memory efficient variant of our algorithm for the computation of $C_{1600}H_{322}$, explaining the comparatively high increase in wall clock time for this step.

The excellent scaling behavior of our method for relatively small systems is also reflected in the early crossover point with respect to canonical SOS-PARI-MP2; for $C_{10}H_{22}$, the SOS-AO-PARI-MP2 energy correction alone is computed in 45 s on the TZP-level of theory, while the respective canonical calculation already takes 93 s.

On the example of $C_{40}H_{82}$ in the TZP basis, we give an estimate on the efficiency of our parallelization strategy: Comparing wall clock times obtained with 1, 8, and 24 cores on the same node, we find parallel speedups of 6.4 and 15.8, respectively. Parallel timing results are also presented for stacks of backbone-free DNA in Table 6.

Table 6. CPU Times and Scaling Behavior with Respect to the Systems Size Relative to the Previous Calculation (in Parentheses) in Terms of the Polynomial Coefficient x in N^x for SOS-AO-PARI-MP2 Calculations on Backbone-Free DNA Stacks on the TZP/*Normal* Level of Theory (All Calculations on a Single Node with 24 Cores, All Timings in min)

no. of units	no. of bf	total		MP2 alone		MP2 time [% of full calc]
1	848	4.1		0.7		17.1
2	1696	20.1	(2.29)	4.3	(2.62)	21.2
4	3392	79.7	(1.99)	20.9	(2.28)	26.2
6	5088	185.1	(2.08)	52.1	(2.25)	28.1

Here, each unit consists of an adenine−guanine and a cytosine−thymine base pair, separated by 3.4 Å. Although these systems are still spatially extended, they are considerably more compact as linear alkanes. For the largest of these systems considered here with 354 atoms and 5088 basis functions, the SOS-AO-PARI-MP2 energy can be evaluated in approximately 3 h on a single compute node, with the computation of the SOS-MP2 energy only accounting for 28% of the total elapsed time. Although the overall scaling is slightly worse than for the linear alkane chains, one still discovers the onset of subquadratic scaling for the whole calculation and convergence to quadratic scaling for the SOS-MP2 calculation only.

The efficiency of our implementation is illustrated on different types of realistic, compact systems (see Figure 5) in Table 7, where we give detailed timings for the most expensive steps of the SOS-AO-PARI-MP2 calculations from Table 2.

The most expensive part for each calculation is the SCF. The wall clock time for the calculation of the SOS-AO-PARI-MP2 energy correction is clearly dominated by step 3a/3b, whereas the cubic scaling evaluation of the PDMs (step 1) is negligible. Step 3a/3b is also the part of our algorithm that would probably profit most from the exploitation of sparsity in the half-transformed fit coefficient tensors. For the very compact systems $(S_8)_{20}$ (compund e in Figure 5) and $Au_{21}S(SCH_3)_{15}$ (f) in Figure 5), the half-transformation of the fit coefficients (step 2a/2b) also consumes a considerable share of the total wall clock time as distance effects do not come into play here. As the majority of the individual tensor contractions scale as $N_b^2N_f^2$ in the SCF and in the MP2 part, the large number of basis functions and auxiliary fit functions for the gold atoms (see Table 1) makes the computation for this system particularly slow. The efficiency of step 6 is more or less independent from the molecular geometry, best seen on the example of the water cluster, indicating that the multipole

https://dx.doi.org/10.1021/acs.jctc.9b00854
J. Chem. Theory Comput. 2020, 16, 875−891

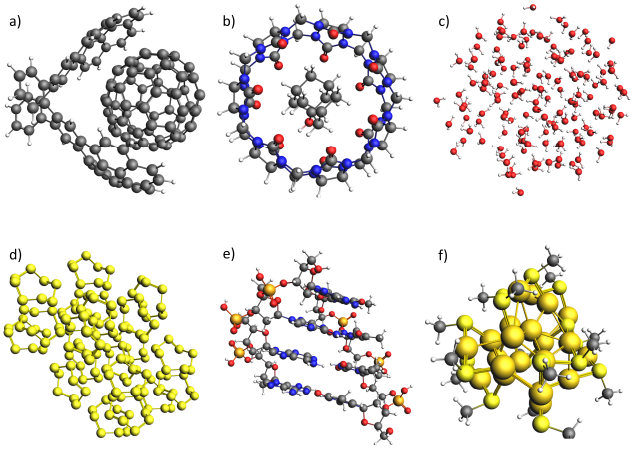

Figure 5. Realistic 3D systems employed in this work. Upper panel from left to right: 4b, 7b from the S30L testset of Grimme and co-workers,[224] and a $(H_2O)_{142}$ water cluster[156] from the Ochsenfeld benchmark set. Lower panel from left to right: A $(S_8)_{20}$ sulfur cluster,[156] a DNA segment from adenine−thymine base pairs[159] (both from the Ochsenfeld benchmark set), and a substituted cluster of 21 Au atoms from Jones et al.[225]

expansion does not lead to large computational savings for these compact systems.

In the end, we comment on the memory requirements of our code. The computation of the SOS-AO-PARI-MP2 energy for $C_{160}H_{322}$ in TZ2P quality with roughly 8500 AOs could only been achieved by using our more memory efficient implementation, even when 128 GB memory is used and calculations on even larger systems are impossible due to the memory requirements of the SCF. Although we do not think that molecules of this size will be the main target of our implementation, this is currently a severe drawback of our algorithm and we are planning further optimization in this direction.

4. CONCLUSION

We have demonstrated on test sets of collectively 187 data points that dimerization energies and conformational energies from PARI-MP2 deviate from their DF-MP2/CBS counterparts by less than 1 kcal/mol on average, when non-correlation consistent STO-type basis sets of triple-ζ quality and our default auxiliary fit sets are used. We have also demonstrated the accuracy of this approach for large systems of more than 100 atoms and shown that our implementation reproduces CCSD(T)/CBS reference values better than DF-MP2/CBS for the HEAVY28 test set of noncovalent interaction energies between heavy element hydrides when relativistic effects are approximated on the ZORA/MAPA level.

Comparison to DF-MP2 calculations on the S66 test set shows that the error of our calculations is of the same order of magnitude as the basis set incompleteness error of GTO-type basis sets of comparable size. The maximum deviation observed is below 4 kcal/mol for the TZP basis set with only a single polarization function per atom and considerably lower than 1 kcal/mol for some of the investigated test sets. We expect significant improvement of these values by employing fit sets optimized for correlation methods as it is common practice for DF-MP2 with GTOs.[142,226−228] To the best of our knowledge, such fit sets have not been designed for STO based PARI yet and research in this direction is currently being pursued by our group.

Additionally, we have presented a quadratic scaling SOS-AO-PARI-MP2 algorithm. The overall evaluation of the SOS-MP2 energy scales quadratically and the post-SCF energy correction is computed considerably faster than the SCF itself for all system considered herein. Among others, we have demonstrated the efficiency of our approach on a very compact cluster of 160 sulfur atoms with 4480 basis functions, and a cluster of 142 water molecules with 4544 basis functions: Each all-electron calculation could be performed in approximately 3 h on a single compute node. Another attractive feature of our implementation is its early crossover to canonical SOS-PARI-MP2 in terms of wall clock time: For a linear alkane chain with only 10 carbon atoms, our AO based algorithm is already twice as fast as our MO based one. As a consequence, our algorithm is fast for medium and large compact systems of up to several hundreds of atoms, the bottleneck, with regard to both memory and wall clock time, being the SCF rather than the MP2 calculation. As we are mostly avoiding disk I/O, our approach is particularly appealing if the calculations are run on a machine with relatively slow disks, such as the nowadays ubiquitous computer clusters with external storage devices.

At the moment, the post-SCF energy correction does not scale as favorably as the SCF itself. Using sparse matrix algebra, we could possibly turn our current implementation into a truly linear scaling one. However, one might legitimately argue that this would not bring much additional value. Even if one could speed up the MP2 calculation alone by a factor of 2, the overall

Table 7. Detailed Wall Clock Times (in min) for SOS-AO-PARI-MP2 Calculations on Selected Realistic 3D Systems on the TZP/*Normal* Level of Theory on a Single Node with 24 Cores[a]

	4b	7b	$(H_2O)_{142}$	DNA_4	$(S_8)_{20}$	$Au_{21}S(SCH_3)_{15}$[b,c]
no. of atoms	158	153	426	260	160	97
no. of bf	2768	2248	4544	3638	4480	2414
			Timings			
total	76.2	40.3	186.0	104.3	177.9	269.2
total MP2	15.6	9.4	56.7	28.7	75.5	106.7
step 1[d]	0.06	0.04	0.21	0.10	0.19	0.05
step 2a/2b	2.4	1.4	6.63	3.6	11.8	19.62
step 3a/3b	10.0	5.7	36.0	16.4	49.6	75.6
step 6	2.2	1.6	18.0	6.8	6.2	6.3

[a]The first two structures are taken from the S30L test set,[224] structures 3−5 are from the test set of Ochsenfeld and co-workers[156,159] and the structure of the last molecule has been taken from Jones et al.[225] [b]Relativistic effects have been treated on the ZORA/MAPA level of theory. [c]Due to the small HOMO−LUMO gap, N_{nq} = 8 was chosen. [d]Numbering of steps refers to Table 2.

https://dx.doi.org/10.1021/acs.jctc.9b00854
J. Chem. Theory Comput. 2020, 16, 875−891

wall clock time for the computation of the SOS-MP2 energy for the sulfur cluster (where the MP2 is particularly slow compared to the SCF) would only be reduced by 20%. In other words, major efficiency gains can only be achieved when the bottleneck of the computation, the computation of the exact exchange in the SCF, is optimized.

Although larger computational savings could possibly be achieved for systems much larger than the ones presented herein, we do not think that even then these large systems would be a probable target of our algorithm. Furthermore, application of our algorithm to these systems is hampered by its rather unfavorable memory requirements (if one wants to avoid disk I/O) and further development of the code will rather focus on improvements in this direction. We are also planning to extend our implementation to periodic systems and to implement gradients as well.

Although we think that accurate and fast MP2 correlation energies are highly desirable in themselves, they are arguably most relevant in the framework of double-hybrid density functional approximations. At the moment, we are working on a comprehensive benchmark of state-of-the-art SOS based double hybrids for small as well as for large molecules. As shown only recently,[127] this class of double hybrids is in almost all cases not inferior to SCS-MP2 based ones, especially if the recently developed D4 extension[229,230] to the D3 dispersion correction[219,231,232] is used.

■ ASSOCIATED CONTENT

Supporting Information

The Supporting Information is available free of charge at https://pubs.acs.org/doi/10.1021/acs.jctc.9b00854.

Exponents of all auxiliary fit functions used in our calculations, individual reaction energies referred to herein as well as bonding energies with respect to atomic fragments for all single-point calculations performed, all structures used for the calculations in this work; all information related to the computed energies in CSV format (ZIP)

■ AUTHOR INFORMATION

Corresponding Author

Arno Förster − *Theoretical Chemistry, Vrije Universiteit, NL-1081 HV Amsterdam, The Netherlands;* orcid.org/0000-0002-0957-4081; Email: a.t.l.foerster@vu.nl

Authors

Mirko Franchini − *Theoretical Chemistry, Vrije Universiteit, NL-1081 HV Amsterdam, The Netherlands; Scientific Computing & Modelling NV, NL-1081 HV Amsterdam, The Netherlands*

Erik van Lenthe − *Scientific Computing & Modelling NV, NL-1081 HV Amsterdam, The Netherlands*

Lucas Visscher − *Theoretical Chemistry, Vrije Universiteit, NL-1081 HV Amsterdam, The Netherlands;* orcid.org/0000-0002-7748-6243

Complete contact information is available at: https://pubs.acs.org/10.1021/acs.jctc.9b00854

Notes

The authors declare no competing financial interest.

■ ACKNOWLEDGMENTS

This research received funding from The Netherlands Organisation for Scientific Research (NWO) in the framework of the Innovation Fund for Chemistry and from the Ministry of Economic Affairs in the framework of the "*TKI/PPS-Toeslagregeling*".

■ REFERENCES

(1) Rubensson, E. H.; Rudberg, E.; Salek, P. *Linear-Scaling Techniques in Computational Chemistry and Physics*; Springer, 2011; pp 263−300.

(2) Kohn, W.; Sham, L. J. Self-Consistent Equations Including Exchange and Correlation Effects. *Phys. Rev.* **1965**, *140*, A1133.

(3) Hohenberg, P.; Kohn, W. Inhomogeneous Electron Gas. *Phys. Rev.* **1964**, *136*, 864−871.

(4) Levy, M. Universal variational functionals of electron densities, first-order density matrices, and natural spin-orbitals and solution of the v-representability problem. *Proc. Natl. Acad. Sci. U. S. A.* **1979**, *76*, 6062−6065.

(5) Cohen, A. J.; Mori-Sánchez, P.; Yang, W. Challenges for Density Functional Theory. *Chem. Rev.* **2012**, *112*, 289−320.

(6) Pribram-Jones, A.; Gross, D. A.; Burke, K. DFT: A Theory Full of Holes? *Annu. Rev. Phys. Chem.* **2015**, *66*, 283−304.

(7) Becke, A. D. Perspective: Fifty years of density-functional theory in chemical physics. *J. Chem. Phys.* **2014**, *140*, 18A301.

(8) Jones, R. O. Density functional theory: Its origins, rise to prominence, and future. *Rev. Mod. Phys.* **2015**, *87*, 897.

(9) Mardirossian, N.; Head-Gordon, M. Thirty years of density functional theory in computational chemistry: An overview and extensive assessment of 200 density functionals. *Mol. Phys.* **2017**, *115*, 2315−2372.

(10) Gould, T. What Makes a Density Functional Approximation Good? Insights from the Left Fukui Function. *J. Chem. Theory Comput.* **2017**, *13*, 2373−2377.

(11) Goerigk, L.; Mehta, N. A Trip to the Density Functional Theory Zoo: Warnings and Recommendations for the User. *Aust. J. Chem.* **2019**, *72*, 563.

(12) Becke, A. D. Density functional calculations of molecular bond energies. *J. Chem. Phys.* **1986**, *84*, 4524−4529.

(13) Becke, A. D. Density-functional thermochemistry. III. The role of exact exchange. *J. Chem. Phys.* **1993**, *98*, 5648−5652.

(14) Johnson, E. R.; Wolkow, R. A.; Dilabio, G. A. Application of 25 density functionals to dispersion-bound homomolecular dimers. *Chem. Phys. Lett.* **2004**, *394*, 334−338.

(15) Sousa, S. F.; Fernandes, P. A.; Ramos, M. J. General performance of density functionals. *J. Phys. Chem. A* **2007**, *111*, 10439−10452.

(16) Schreiner, P. R. Relative energy computations with approximate density functional theory - A caveat! *Angew. Chem., Int. Ed.* **2007**, *46*, 4217−4219.

(17) Zhao, Y.; Truhlar, D. G. Density Functionals with Broad Applicability in Chemistry. *Acc. Chem. Res.* **2008**, *41*, 157−167.

(18) Boese, A. D. Density functional theory and hydrogen bonds: Are we there yet? *ChemPhysChem* **2015**, *16*, 978−985.

(19) Hollman, D. S.; Simmonett, A. C.; Schaefer, H. F. The benzene +OH potential energy surface: Intermediates and transition states. *Phys. Chem. Chem. Phys.* **2011**, *13*, 2214−2221.

(20) Hohenstein, E. G.; Parrish, R. M.; Sherrill, C. D.; Turney, J. M.; Schaefer, H. F. Large-scale symmetry-adapted perturbation theory computations via density fitting and Laplace transformation techniques: Investigating the fundamental forces of DNA-intercalator interactions. *J. Chem. Phys.* **2011**, *135*, 174107.

(21) de la Roza, A. O.; DiLabio, G. A. *Non-covalent Interactions in Quantum Chemistry and Physics: Theory and Applications*; Elsevier Inc., 2017.

(22) The notion of N^x always implies $O(N^x)$. That is, the function f, mapping the system size to the runtime of an algorithm, does not grow asymptotically faster than N^x.

(23) Møller, C.; Plesset, M. Note on an Approximation Treatment for Many-Electron Systems. *Phys. Rev.* **1934**, *46*, 618−622.
(24) Čížek, J.; Paldus, J. Correlation problems in atomic and molecular systems III. Rederivation of the coupled-pair many-electron theory using the traditional quantum chemical methodst. *Int. J. Quantum Chem.* **1971**, *5*, 359−379.
(25) Purvis, G. D.; Bartlett, R. J. A full coupled-cluster singles and doubles model: The inclusion of disconnected triples. *J. Chem. Phys.* **1982**, *76*, 1910−1918.
(26) Bartlett, R. J. Coupled-cluster approach to molecular structure and spectra: A step toward predictive quantum chemistry. *J. Phys. Chem.* **1989**, *93*, 1697−1708.
(27) Raghavachari, K.; Trucks, G.; Pople, John A.; Head-Gordon, M. A fifth-order perturbation comparison of electron correlation theories. *Chem. Phys. Lett.* **1989**, *157*, 479−483.
(28) Neese, F.; Wennmohs, F.; Hansen, A. Efficient and accurate local approximations to coupled-electron pair approaches: An attempt to revive the pair natural orbital method. *J. Chem. Phys.* **2009**, *130*, 114108.
(29) Klopper, W.; Manby, F. R.; Ten-No, S.; Valeev, E. F. R12 methods in explicitly correlated molecular electronic structure theory. *Int. Rev. Phys. Chem.* **2006**, *25*, 427−468.
(30) Boys, S. F. Construction of some molecular orbitals to be approximately invariant for changes from one molecule to another. *Rev. Mod. Phys.* **1960**, *32*, 296−299.
(31) Pipek, J.; Mezey, P. G. A fast intrinsic localization procedure applicable for ab initio and semiempirical linear combination of atomic orbital wave functions. *J. Chem. Phys.* **1989**, *90*, 4916−4926.
(32) Guo, Y.; Li, W.; Li, S. An efficient linear scaling procedure for constructing localized orbitals of large molecules based on the one-particle density matrix. *J. Chem. Phys.* **2011**, *135*, 134107.
(33) Høyvik, I. M.; Jansik, B.; Jørgensen, P. Orbital localization using fourth central moment minimization. *J. Chem. Phys.* **2012**, *137*, 224114.
(34) Høyvik, I. M.; Jansik, B.; Jørgensen, P. Trust region minimization of orbital localization functions. *J. Chem. Theory Comput.* **2012**, *8*, 3137−3146.
(35) Høyvik, I. M.; Jansik, B.; Jørgensen, P. Pipek-Mezey localization of occupied and virtual orbitals. *J. Comput. Chem.* **2013**, *34*, 1456−1462.
(36) Høyvik, I. M.; Kristensen, K.; Kjærgaard, T.; Jørgensen, P. A perspective on the localizability of hartree-fock orbitals. *Theor. Chem. Acc.* **2014**, *133*, 1417.
(37) Pulay, P. Localizability of Dynamic Electron Correlation. *Chem. Phys. Lett.* **1983**, *100*, 151−154.
(38) Sæbø, S.; Pulay, P. Local configuration interaction: An efficient approach for larger molecules. *Chem. Phys. Lett.* **1985**, *113*, 13−18.
(39) Pulay, P.; Saebø, S. Orbital-invariant formulation and second-order gradient evaluation in Møller-Plesset perturbation theory. *Theor. Chim. Acta* **1986**, *69*, 357−368.
(40) Saebø, S.; Pulay, P. Fourth-order Mo/ller-Plessett perturbation theory in the local correlation treatment. I. Method. *J. Chem. Phys.* **1987**, *86*, 914−922.
(41) Saebo, S.; Pulay, P. The local correlation treatment. II. Implementation and tests. *J. Chem. Phys.* **1988**, *88*, 1884−1890.
(42) Hampel, C.; Werner, H. J. Local treatment of electron correlation in coupled cluster theory. *J. Chem. Phys.* **1996**, *104*, 6286−6297.
(43) Schütz, M.; Werner, H. J. Local perturbative triples correction (T) with linear cost scaling. *Chem. Phys. Lett.* **2000**, *318*, 370−378.
(44) Schütz, M. Low-order scaling local electron correlation methods. V. Connected triples beyond (T): Linear scaling local CCSDT-1b. *J. Chem. Phys.* **2002**, *116*, 8772−8785.
(45) Werner, H. J.; Manby, F. R.; Knowles, P. J. Fast linear scaling second-order Møller-Plesset perturbation theory (MP2) using local and density fitting approximations. *J. Chem. Phys.* **2003**, *118*, 8149−8160.
(46) Schütz, M.; Manby, F. R. Linear scaling local coupled cluster theory with density fitting. Part I: 4-external integrals. *Phys. Chem. Chem. Phys.* **2003**, *5*, 3349−3358.
(47) Korona, T.; Werner, H. J. Local treatment of electron excitations in the EOM-CCSD method. *J. Chem. Phys.* **2003**, *118*, 3006−3019.
(48) Werner, H. J.; Manby, F. R. Explicitly correlated second-order perturbation theory using density fitting and local approximations. *J. Chem. Phys.* **2006**, *124*, 054114.
(49) Kats, D.; Korona, T.; Schütz, M. Local CC2 electronic excitation energies for large molecules with density fitting. *J. Chem. Phys.* **2006**, *125*, 104106.
(50) Doser, B; Lambrecht, D. S.; Ochsenfeld, C. Tighter multipole-based integral estimates and parallel implementation of linear-scaling AO−MP2 theory. *Phys. Chem. Chem. Phys.* **2008**, *10*, 3335−3344.
(51) El Azhary, A.; Rauhut, G.; Pulay, P.; Werner, H. J. Analytical energy gradients for local second-order Møller-Plesset perturbation theory. *J. Chem. Phys.* **1998**, *108*, 5185−5193.
(52) Hetzer, G.; Pulay, P.; Werner, H. J. Multipole approximation of distant pair energies in local MP2 calculations. *Chem. Phys. Lett.* **1998**, *290*, 143−149.
(53) Schütz, M.; Hetzer, G.; Werner, H. J. Low-order scaling local electron correlation methods. I. Linear scaling local MP2. *J. Chem. Phys.* **1999**, *111*, 5691−5705.
(54) Schütz, M.; Werner, H. J.; Lindh, R.; Manby, F. R. Analytical energy gradients for local second-order Møller-Plesset perturbation theory using density fitting approximations. *J. Chem. Phys.* **2004**, *121*, 737−750.
(55) Kurashige, Y.; Yang, J.; Chan, G. K.; Manby, F. R. Optimization of orbital-specific virtuals in local Møller-Plesset perturbation theory. *J. Chem. Phys.* **2012**, *136*, 124106.
(56) Neese, F.; Hansen, A.; Liakos, D. G. Efficient and accurate approximations to the local coupled cluster singles doubles method using a truncated pair natural orbital basis. *J. Chem. Phys.* **2009**, *131*, 064103.
(57) Kossmann, S.; Neese, F. Correlated ab initio spin densities for larger molecules: Orbital-optimized spin-component-scaled MP2 method. *J. Phys. Chem. A* **2010**, *114*, 11768−11781.
(58) Riplinger, C.; Sandhoefer, B.; Hansen, A.; Neese, F. Natural triple excitations in local coupled cluster calculations with pair natural orbitals. *J. Chem. Phys.* **2013**, *139*, 134101.
(59) Pinski, P.; Riplinger, C.; Valeev, E. F.; Neese, F. Sparse maps - A systematic infrastructure for reduced-scaling electronic structure methods. I. An efficient and simple linear scaling local MP2 method that uses an intermediate basis of pair natural orbitals. *J. Chem. Phys.* **2015**, *143*, 034108.
(60) Yang, J.; Chan, G. K. L.; Manby, F. R.; Schütz, M.; Werner, H. J. The orbital-specific-virtual local coupled cluster singles and doubles method. *J. Chem. Phys.* **2012**, *136*, 144105.
(61) Hättig, C.; Tew, D. P.; Helmich, B. Local explicitly correlated second- and third-order M?ller-Plesset perturbation theory with pair natural orbitals. *J. Chem. Phys.* **2012**, *136*, 204105.
(62) Schmitz, G.; Helmich, B.; Hättig, C. A O(N3) scaling PNO-MP2 method using a hybrid OSV-PNO approach with an iterative direct generation of OSVs. *Mol. Phys.* **2013**, *111*, 2463−2476.
(63) Schütz, M.; Yang, J.; Chan, G. K. L.; Manby, F. R.; Werner, H. J. The orbital-specific virtual local triples correction: OSV-L(T). *J. Chem. Phys.* **2013**, *138*, 054109.
(64) Schmitz, G.; Hättig, C.; Tew, D. P. Explicitly correlated PNO-MP2 and PNO-CCSD and their application to the S66 set and large molecular systems. *Phys. Chem. Chem. Phys.* **2014**, *16*, 22167−22178.
(65) Werner, H. J.; Knizia, G.; Krause, C.; Schwilk, M.; Dornbach, M. Scalable electron correlation methods I.: PNO-LMP2 with linear scaling in the molecular size and near-inverse-linear scaling in the number of processors. *J. Chem. Theory Comput.* **2015**, *11*, 484−507.
(66) Ma, Q.; Werner, H. J. Scalable Electron Correlation Methods. 2. Parallel PNO-LMP2-F12 with Near Linear Scaling in the Molecular Size. *J. Chem. Theory Comput.* **2015**, *11*, 5291−5304.

https://dx.doi.org/10.1021/acs.jctc.9b00854
J. Chem. Theory Comput. 2020, 16, 875−891

(67) Nagy, P. R.; Samu, G.; Kállay, M. An Integral-Direct Linear-Scaling Second-Order Møller-Plesset Approach. *J. Chem. Theory Comput.* **2016**, *12*, 4897−4914.
(68) Ma, Q.; Schwilk, M.; Köppl, C.; Werner, H. J. Scalable Electron Correlation Methods. 4. Parallel Explicitly Correlated Local Coupled Cluster with Pair Natural Orbitals (PNO-LCCSD-F12). *J. Chem. Theory Comput.* **2017**, *13*, 4871−4896.
(69) Nagy, P. R.; Kállay, M. Optimization of the linear-scaling local natural orbital CCSD(T) method: Redundancy-free triples correction using Laplace transform. *J. Chem. Phys.* **2017**, *146*, 214106.
(70) Ahlrichs, R.; Kutzelnigg, W. Ab initio calculations on small hydrides including electron correlation - I. The BeH2 molecule in its ground state. *Theor. Chim. Acta* **1968**, *10*, 377−387.
(71) Jungen, M.; Ahlrichs, R. Ab initio calculations on small hydrides including electron correlation - III. A study of the valence shell intrapair and interpair correlation energy of some first row hydrides. *Theor. Chim. Acta* **1970**, *17*, 339−347.
(72) Meyer, W. Ionization energies of water from PNO-CI calculations. *Int. J. Quantum Chem.* **1971**, *5*, 341−348.
(73) Meyer, W. PNO-CI and CEPA studies of electron correlation effects - II. Potential curves and dipole moment functions of the OH radical. *Theor. Chim. Acta* **1974**, *35*, 277−292.
(74) Ahlrichs, R.; Driessler, F.; Lischka, H.; Staemmler, V.; Kutzelnigg, W. PNO-CI (pair natural orbital configuration interaction) and CEPA-PNO (coupled electron pair approximation with pair natural orbitals) calculations of molecular systems. II. The molecules BeH2, BH, BH3, CH4, CH3-, NH3 (planar and pyramidal), H2O, OH3+, HF. *J. Chem. Phys.* **1975**, *62*, 1235−1247.
(75) Taylor, P. R.; Bacskay, G. B.; Hush, N. S.; Hurley, A. C. The coupled-pair approximation in a basis of independent-pair natural orbitals. *Chem. Phys. Lett.* **1976**, *41*, 444−449.
(76) Rosmus, P.; Meyer, W. PNO-CI and CEPA studies of electron correlation effects. VI. Electron affinities of the first-row and second-row diatomic hydrides and the spectroscopic constants of their negative ions. *J. Chem. Phys.* **1978**, *69*, 2745−2751.
(77) Taylor, P. R.; Bacskay, G. B.; Hush, N. S.; Hurley, A. C. Unlinked cluster effects in molecular electronic structure. I. The HCN and HNC molecules. *J. Chem. Phys.* **1978**, *69*, 1971−1979.
(78) Ahlrichs, R. Many body perturbation calculations and coupled electron pair models. *Comput. Phys. Commun.* **1979**, *17*, 31−45.
(79) Taylor, P. R. A rapidly convergent Cl expansion based on several reference configurations, using optimized correlating orbitals. *J. Chem. Phys.* **1981**, *74*, 1256−1270.
(80) Staemmler, V.; Jaquet, R. CEPA calculations on open-shell molecules. I. Outline of the method. *Theor. Chim. Acta* **1981**, *59*, 487−500.
(81) Koch, S.; Kutzelnigg, W. Comparison of CEPA and CP-MET methods. *Theor. Chim. Acta* **1980**, *59*, 387−411.
(82) Ahlrichs, R.; Scharf, P.; Ehrhardt, C. The coupled pair functional (CPF). A size consistent modification of the CI(SD) based on an energy functional. *J. Chem. Phys.* **1985**, *82*, 890−898.
(83) Pulay, P.; Saebø, S. Variational CEPA: Comparison with different Many-Body Methods. *Chem. Phys. Lett.* **1985**, *117*, 37−41.
(84) Edmiston, C.; Krauss, M. Configuration-Interaction Calculation of H3 and H2. *J. Chem. Phys.* **1965**, *42*, 1119−1120.
(85) Edmiston, C.; Ruedenberg, K. Localized Atomic and Molecular Orbitals. II. *J. Chem. Phys.* **1965**, *43*, 97−116.
(86) Friedrich, J.; Hanrath, M.; Dolg, M. Fully automated implementation of the incremental scheme: Application to CCSD energies for hydrocarbons and transition metal compounds. *J. Chem. Phys.* **2007**, *126*, 154110.
(87) Friedrich, J.; Dolg, M. Fully Automated Incremental Evaluation of MP2 and CCSD(T) Energies: Application to Water Clusters. *J. Chem. Theory Comput.* **2009**, *5*, 287−294.
(88) Raghavachari, K.; Saha, A. Accurate Composite and Fragment based Quantum Chemical Models for Large Molecules. *Chem. Rev.* **2015**, *115*, 5643−5677.
(89) Li, W.; Piecuch, P.; Gour, J. R.; Li, S. Local correlation calculations using standard and renormalized coupled-cluster approaches. *J. Chem. Phys.* **2009**, *131*, 114109.
(90) Rolik, Z.; Szegedy, L.; Ladjánszki, I.; Ladóczki, B.; Kállay, M. An efficient linear-scaling CCSD(T) method based on local natural orbitals. *J. Chem. Phys.* **2013**, *139*, 094105.
(91) Kállay, M. Linear-scaling implementation of the direct random-phase approximation. *J. Chem. Phys.* **2015**, *142*, 204105.
(92) Yang, Weitao Direct Calculation of Electron Density in Density-Functional Theory. *Phys. Rev. Lett.* **1991**, *66*, 1438−1441.
(93) Yang, W.; Lee, T. S. A density-matrix divide-and-conquer approach for electronic structure calculations of large molecules. *J. Chem. Phys.* **1995**, *103*, 5674−5678.
(94) Li, W.; Li, S. Divide-and-conquer local correlation approach to the correlation energy of large molecules. *J. Chem. Phys.* **2004**, *121*, 6649−6657.
(95) Flocke, N.; Bartlett, R. J. A natural linear scaling coupled-cluster method. *J. Chem. Phys.* **2004**, *121*, 10935−10944.
(96) Kobayashi, M.; Imamura, Y.; Nakai, H. Alternative linear-scaling methodology for the second-order Møller-Plesset perturbation calculation based on the divide-and-conquer method. *J. Chem. Phys.* **2007**, *127*, 074103.
(97) Kobayashi, M.; Nakai, H. Extension of linear-scaling divide-and-conquer based correlation method to coupled cluster theory with singles and doubles excitations. *J. Chem. Phys.* **2008**, *129*, 044103.
(98) Kobayashi, M.; Nakai, H. Divide-and-conquer based linear-scaling approach for traditional and renormalized coupled cluster methods with single, double, and noniterative triple excitations. *J. Chem. Phys.* **2009**, *131*, 114108.
(99) Ziółkowski, M.; Jansík, B.; Kjrgaard, T.; Jørgensen, P. Linear scaling coupled cluster method with correlation energy based error control. *J. Chem. Phys.* **2010**, *133*, 014107.
(100) Kristensen, K.; Ziółkowski, M.; Jansík, B.; Kjærgaard, T.; Jørgensen, P. A locality analysis of the divide-expand-consolidate coupled cluster amplitude equations. *J. Chem. Theory Comput.* **2011**, *7*, 1677−1694.
(101) Kristensen, K.; Jorgensen, P.; Jansík, B.; Kjærgaard, T.; Reine, S. Molecular gradient for second-order Møller-Plesset perturbation theory using the divide-expand-consolidate (DEC) scheme. *J. Chem. Phys.* **2012**, *137*, 114102.
(102) Høyvik, I. M.; Kristensen, K.; Jansik, B.; Jrgensen, P. The divide-expand-consolidate family of coupled cluster methods: Numerical illustrations using second order Møller-Plesset perturbation theory. *J. Chem. Phys.* **2012**, *136*, 014105.
(103) Kristensen, K.; Kjærgaard, T.; Høyvik, I. M.; Ettenhuber, P.; Jørgensen, P.; Jansik, B.; Reine, S.; Jakowski, J. The divide-expand-consolidate MP2 scheme goes massively parallel. *Mol. Phys.* **2013**, *111*, 1196−1210.
(104) Eriksen, J. J.; Baudin, P.; Ettenhuber, P.; Kristensen, K.; Kjærgaard, T.; Jørgensen, P. Linear-Scaling Coupled Cluster with Perturbative Triple Excitations: The Divide-Expand-Consolidate CCSD(T) Model. *J. Chem. Theory Comput.* **2015**, *11*, 2984−2993.
(105) Baudin, P.; Ettenhuber, P.; Reine, S.; Kristensen, K.; Kjærgaard, T. Efficient linear-scaling second-order Møller-Plesset perturbation theory: The divide-expand-consolidate RI-MP2 model. *J. Chem. Phys.* **2016**, *144*, 054102.
(106) Kjærgaard, T. The Laplace transformed divide-expand-consolidate resolution of the identity second-order Møller-Plesset perturbation (DEC-LT-RIMP2) theory method. *J. Chem. Phys.* **2017**, *146*, 044103.
(107) Nagy, P. R.; Samu, G.; Kállay, M. Optimization of the Linear-Scaling Local Natural Orbital CCSD(T) Method: Improved Algorithm and Benchmark Applications. *J. Chem. Theory Comput.* **2018**, *14*, 4193−4215.
(108) Jurečka, P.; Šponer, J.; Černý, J.; Hobza, P. Benchmark database of accurate (MP2 and CCSD(T) complete basis set limit) interaction energies of small model complexes, DNA base pairs, and amino acid pairs. *Phys. Chem. Chem. Phys.* **2006**, *8*, 1985−1993.

https://dx.doi.org/10.1021/acs.jctc.9b00854
J. Chem. Theory Comput. 2020, 16, 875−891

(109) Zhao, Y.; Truhlar, D. G. Density functionals for noncovalent interaction energies of biological importance. *J. Chem. Theory Comput.* **2007**, *3*, 289−300.
(110) Gauss, J. Effects of electron correlation in the calculation of nuclear magnetic resonance chemical shifts. *J. Chem. Phys.* **1993**, *99*, 3629−3643.
(111) Shelton, D. P.; Rice, J. E. Measurements and Calculations of the Hyperpolarizabilities of Atoms and Small Molecules in the Gas Phase. *Chem. Rev.* **1994**, *94*, 3−29.
(112) Friese, D. H.; Winter, N. O. C.; Balzerowski, P.; Schwan, R.; Hättig, C. Large scale polarizability calculations using the approximate coupled cluster model CC2 and MP2 combined with the resolution-of-the-identity approximation. *J. Chem. Phys.* **2012**, *136*, 174106.
(113) Burns, L. A.; Marshall, M. S.; Sherrill, C. D. Appointing silver and bronze standards for noncovalent interactions: A comparison of spin-component-scaled (SCS), explicitly correlated (F12), and specialized wavefunction approaches. *J. Chem. Phys.* **2014**, *141*, 234111.
(114) Kesharwani, M. K.; Karton, A.; Martin, J. M. Benchmark ab Initio Conformational Energies for the Proteinogenic Amino Acids through Explicitly Correlated Methods. Assessment of Density Functional Methods. *J. Chem. Theory Comput.* **2016**, *12*, 444−454.
(115) Grimme, S. Improved second-order Møller-Plesset perturbation theory by separate scaling of parallel- and antiparallel-spin pair correlation energies. *J. Chem. Phys.* **2003**, *118*, 9095−9102.
(116) Jung, Y.; Lochan, R. C.; Dutoi, A. D.; Head-Gordon, M. Scaled opposite-spin second order moller-plesset correlation energy: An economical electronic structure method. *J. Chem. Phys.* **2004**, *121*, 9793−9802.
(117) Lochan, R. C.; Jung, Y.; Head-Gordon, M. Scaled opposite spin second order Møller-Plesset theory with improved physical description of long-range dispersion interactions. *J. Phys. Chem. A* **2005**, *109*, 7598−7605.
(118) Janesko, B. G.; Scuseria, G. E. Coulomb-only second-order perturbation theory in long-range-corrected hybrid density functionals. *Phys. Chem. Chem. Phys.* **2009**, *11*, 9677−9686.
(119) Grimme, S. Semiempirical hybrid density functional with perturbative second-order correlation. *J. Chem. Phys.* **2006**, *124*, 034108.
(120) Grimme, S.; Mück-Lichtenfeld, C.; Würthwein, E. U.; Ehlers, A. W.; Goumans, T. P.; Lammertsma, K. Consistent theoretical description of 1,3-dipolar cycloaddition reactions. *J. Phys. Chem. A* **2006**, *110*, 2583−2586.
(121) Schwabe, T.; Grimme, S. Towards chemical accuracy for the thermodynamics of large molecules: New hybrid density functionals including non-local correlation effects. *Phys. Chem. Chem. Phys.* **2006**, *8*, 4398−4401.
(122) Grimme, S.; Steinmetz, M.; Korth, M. How to compute isomerization energies of organic molecules with quantum chemical methods. *J. Org. Chem.* **2007**, *72*, 2118−2126.
(123) Kossmann, S.; Kirchner, B.; Neese, F. Performance of modern density functional theory for the prediction of hyperfine structure: Meta-GGA and double hybrid functionals. *Mol. Phys.* **2007**, *105*, 2049−2071.
(124) Neese, F.; Schwabe, T.; Grimme, S. Analytic derivatives for perturbatively corrected "double hybrid" density functionals: Theory, implementation, and applications. *J. Chem. Phys.* **2007**, *126*, 124115.
(125) Tarnopolsky, A.; Karton, A.; Sertchook, R.; Vuzman, D.; Martin, J. M. L. Double-hybrid functional for thermochemical kinetics. *J. Phys. Chem. A* **2008**, *112*, 3−8.
(126) Goerigk, L.; Grimme, S. Double-hybrid density functionals. *Wiley Interdiscip. Rev. Comput. Mol. Sci.* **2014**, *4*, 576−600.
(127) Santra, G.; Sylvetsky, N.; Martin, J. M. Minimally Empirical Double-Hybrid Functionals Trained against the GMTKN55 Database: RevDSD-PBEP86-D4, revDOD-PBE-D4, and DOD-SCAN-D4. *J. Phys. Chem. A* **2019**, *123*, 5129−5143.
(128) We follow the usual practice of referring to multi-index arrays with *n* indices as *n*th-order tensors, irrespective of the transformation properties of these quantities.
(129) Baerends, E. J.; Ellis, D. E.; Ros, P. Self-consistent molecular Hartree-Fock-Slater calculations I. The computational procedure. *Chem. Phys.* **1973**, *2*, 41−51.
(130) Whitten, J. L. Coulombic potential energy integrals and approximations. *J. Chem. Phys.* **1973**, *58*, 4496−4501.
(131) Sambe, H.; Felton, R. H. A new computational approach to Slater's SCF-Xα equation. *J. Chem. Phys.* **1975**, *62*, 1122−1126.
(132) Dunlap, B. I.; Connolly, J. W.; Sabin, J. R. On some approximations in applications of Xα theory. *J. Chem. Phys.* **1979**, *71*, 3396−3402.
(133) Dunlap, B. I.; Connolly, J. W.; Sabin, J. R. On first-row diatomic molecules and local density models. *J. Chem. Phys.* **1979**, *71*, 4993−4999.
(134) Van Alsenoy, C. Ab initio calculations on large molecules: The multiplicative integral approximation. *J. Comput. Chem.* **1988**, *9*, 620−626.
(135) Te Velde, G.; Baerends, E. J. Precise density-functional method for periodic structures. *Phys. Rev. B: Condens. Matter Mater. Phys.* **1991**, *44*, 7888−7903.
(136) Vahtras, O.; Almlöf, J.; Feyereisen, M. W. Integral approximations for LCAO-SCF calculations. *Chem. Phys. Lett.* **1993**, *213*, 514−518.
(137) Guerra, C. F.; Snijders, J. G.; te Velde, G.; Baerends, E. J. Towards an order-N DFT method. *Theor. Chem. Acc.* **1998**, *99*, 391−403.
(138) Dunlap, B. I. Robust and variational fitting: Removing the four-center integrals from center stage in quantum chemistry. *J. Mol. Struct.: THEOCHEM* **2000**, *529*, 37−40.
(139) Dunlap, B. I. Robust and variational fitting. *Phys. Chem. Chem. Phys.* **2000**, *2*, 2113−2116.
(140) Dunlap, B. I.; Rösch, N.; Trickey, S. B. Variational fitting methods for electronic structure calculations. *Mol. Phys.* **2010**, *108*, 3167−3180.
(141) Feyereisen, M.; Fitzgerald, G.; Komornicki, A. Use of approximate integrals in ab initio theory. An application in MP2 energy calculations. *Chem. Phys. Lett.* **1993**, *208*, 359−363.
(142) Weigend, F.; Häser, M.; Patzelt, H.; Ahlrichs, R. RI-MP2: Optimized auxiliary basis sets and demonstration of efficiency. *Chem. Phys. Lett.* **1998**, *294*, 143−152.
(143) Nakajima, T.; Hirao, K. An approximate second-order Møller-Plesset perturbation approach for large molecular calculations. *Chem. Phys. Lett.* **2006**, *427*, 225−229.
(144) Maschio, L.; Usvyat, D.; Manby, F. R.; Casassa, S.; Pisani, C.; Schütz, M. Fast local-MP2 method with density-fitting for crystals. I. Theory and algorithms. *Phys. Rev. B: Condens. Matter Mater. Phys.* **2007**, *76*, 075101.
(145) Vogt, L.; Olivares-Amaya, R.; Kermes, S.; Shao, Y.; Amador-Bedolla, C.; Aspuru-Guzik, A. Accelerating Resolution-of-the-Identity Second-Order Møller-Plesset Quantum Chemistry Calculations with Graphical Processing Units. *J. Phys. Chem. A* **2008**, *112*, 2049−2057.
(146) Ren, X.; Rinke, P.; Blum, V.; Wieferink, J.; Tkatchenko, A.; Sanfilippo, A.; Reuter, K.; Scheffler, M. Resolution-of-identity approach to Hartree-Fock, hybrid density functionals, RPA, MP2 and GW with numeric atom-centered orbital basis functions. *New J. Phys.* **2012**, *14*, 053020.
(147) Ishikawa, T.; Kuwata, K. RI-MP2 gradient calculation of large molecules using the fragment molecular orbital method. *J. Phys. Chem. Lett.* **2012**, *3*, 375−379.
(148) Katouda, M.; Nakajima, T. MPI/OpenMP hybrid parallel algorithm of resolution of identity second-order Møller-plesset perturbation calculation for massively parallel multicore supercomputers. *J. Chem. Theory Comput.* **2013**, *9*, 5373−5380.
(149) Cooper, B.; Girdlestone, S.; Burovskiy, P.; Gaydadjiev, G.; Averbukh, V.; Knowles, P. J.; Luk, W. Quantum Chemistry in Dataflow: Density-Fitting MP2. *J. Chem. Theory Comput.* **2017**, *13*, 5265−5272.
(150) Almlöf, J. Elimination of energy denominators in Møller-Plesset perturbation theory by a Laplace transform approach. *Chem. Phys. Lett.* **1991**, *181*, 319−320.

https://dx.doi.org/10.1021/acs.jctc.9b00854
J. Chem. Theory Comput. 2020, 16, 875−891

(151) Häser, M.; Almlöf, J. Laplace transform techniques in Møller-Plesset perturbation theory. *J. Chem. Phys.* **1992**, *96*, 489−494.
(152) Haser, M. Moeller-Plesset (MP2) perturbation theory for large molecules. *Theor. Chim. Acta* **1993**, *87*, 147−173.
(153) Häser, M.; Ahlrichs, R. Improvements on the direct SCF method. *J. Comput. Chem.* **1989**, *10*, 104−111.
(154) Lambrecht, D. S.; Ochsenfeld, C. Multipole based integral estimates for the rigorous description of distance dependence in two-electron integrals. *J. Chem. Phys.* **2005**, *123*, 184101.
(155) Lambrecht, D. S.; Doser, B.; Ochsenfeld, C. Rigorous integral screening for electron correlation methods. *J. Chem. Phys.* **2005**, *123*, 184102.
(156) Maurer, S. A.; Lambrecht, D. S.; Flaig, D.; Ochsenfeld, C. Distance-dependent Schwarz based integral estimates for two-electron integrals: Reliable tightness vs. Rigorous upper bounds. *J. Chem. Phys.* **2012**, *136*, 144107.
(157) Ayala, P. Y.; Scuseria, G. E. Linear scaling second-order M? ller-Plesset theory in the atomic orbital basis for large molecular systems. *J. Chem. Phys.* **1999**, *110*, 3660−3671.
(158) Scuseria, G. E.; Ayala, P. Y. Linear scaling coupled cluster and perturbation theories in the atomic orbital basis. *J. Chem. Phys.* **1999**, *111*, 8330−8343.
(159) Doser, B.; Lambrecht, D. S.; Kussmann, J.; Ochsenfeld, C. Linear-scaling atomic orbital based second-order Møller-Plesset perturbation theory by rigorous integral screening criteria. *J. Chem. Phys.* **2009**, *130*, 064107.
(160) Doser, B.; Zienau, J.; Clin, L.; Lambrecht, D. S.; Ochsenfeld, C. A linear-scaling MP2 method for large molecules by rigorous integral-screening criteria. *Z. Phys. Chem.* **2010**, *224*, 397−412.
(161) Maurer, S. A.; Lambrecht, D. S.; Kussmann, J.; Ochsenfeld, C. Efficient distance-including integral screening in linear-scaling Møller-Plesset perturbation theory. *J. Chem. Phys.* **2013**, *138*, 014101.
(162) Maurer, S. A.; Beer, M.; Lambrecht, D. S.; Ochsenfeld, C. Linear-scaling symmetry-adapted perturbation theory with scaled dispersion. *J. Chem. Phys.* **2013**, *139*, 184104.
(163) Pulay, P.; Saebo, S.; Wolinski, K. Efficient calculation of canonical MP2 energies. *Chem. Phys. Lett.* **2001**, *344*, 543−552.
(164) Maurer, S. A.; Kussmann, J.; Ochsenfeld, C. Communication: A reduced scaling J-engine based reformulation of SOS-MP2 using graphics processing units. *J. Chem. Phys.* **2014**, *141*, 051106.
(165) Beebe, N. H.; Linderberg, J. Simplifications in the generation and transformation of two-electron integrals in molecular calculations. *Int. J. Quantum Chem.* **1977**, *12*, 683−705.
(166) Koch, H.; Sánchez De Merás, A.; Pedersen, T. B. Reduced scaling in electronic structure calculations using Cholesky decompositions. *J. Chem. Phys.* **2003**, *118*, 9481−9484.
(167) Aquilante, F.; Lindh, R.; Bondo Pedersen, T. Unbiased auxiliary basis sets for accurate two-electron integral approximations. *J. Chem. Phys.* **2007**, *127*, 114107.
(168) Boman, L.; Koch, H.; Sánchez De Merás, A. Method specific Cholesky decomposition: Coulomb and exchange energies. *J. Chem. Phys.* **2008**, *129*, 134107.
(169) Aquilante, F.; Gagliardi, L.; Pedersen, T. B.; Lindh, R. Atomic Cholesky decompositions: A route to unbiased auxiliary basis sets for density fitting approximation with tunable accuracy and efficiency. *J. Chem. Phys.* **2009**, *130*, 154107.
(170) Schweizer, S.; Doser, B.; Ochsenfeld, C. An atomic orbital based reformulation of energy gradients in second-order Møller-Plesset perturbation theory. *J. Chem. Phys.* **2008**, *128*, 154101.
(171) Zienau, J.; Clin, L.; Doser, B.; Ochsenfeld, C. Cholesky-decomposed densities in laplace based second-order møller-plesset perturbation theory. *J. Chem. Phys.* **2009**, *130*, 204112.
(172) Maurer, S. A.; Clin, L.; Ochsenfeld, C. Cholesky-decomposed density MP2 with density fitting: Accurate MP2 and double-hybrid DFT energies for large systems. *J. Chem. Phys.* **2014**, *140*, 224112.
(173) Vogler, S.; Ludwig, M.; Maurer, M.; Ochsenfeld, C. Low-scaling first-order properties within second-order Møller-Plesset perturbation theory using Cholesky decomposed density matrices. *J. Chem. Phys.* **2017**, *147*, 024101.
(174) Hohenstein, E. G.; Parrish, R. M.; Martínez, T. J. Tensor hypercontraction density fitting. I. Quartic scaling second- and third-order Møller-Plesset perturbation theory. *J. Chem. Phys.* **2012**, *137*, 044103.
(175) Parrish, R. M.; Hohenstein, E. G.; Martínez, T. J.; Sherrill, C. D. Tensor hypercontraction. II. Least-squares renormalization. *J. Chem. Phys.* **2012**, *137*, 224106.
(176) Hohenstein, E. G.; Parrish, R. M.; Sherrill, C. D.; Martínez, T. J. Communication: Tensor hypercontraction. III. Least-squares tensor hypercontraction for the determination of correlated wavefunctions. *J. Chem. Phys.* **2012**, *137*, 221101.
(177) Hohenstein, E. G.; Kokkila, S. I.; Parrish, R. M.; Martínez, T. J. Tensor hypercontraction equation-of-motion second-order approximate coupled cluster: Electronic excitation energies in O (N4) time. *J. Phys. Chem. B* **2013**, *117*, 12972−12978.
(178) Hohenstein, E. G.; Kokkila, S. I.; Parrish, R. M.; Martínez, T. J. Quartic scaling second-order approximate coupled cluster singles and doubles via tensor hypercontraction: THC-CC2. *J. Chem. Phys.* **2013**, *138*, 124111.
(179) Parrish, R. M.; Hohenstein, E. G.; Schunck, N. F.; Sherrill, C. D.; Martínez, T. J. Exact tensor hypercontraction: A universal technique for the resolution of matrix elements of local finite-range N-body potentials in many-body quantum problems. *Phys. Rev. Lett.* **2013**, *111*, 132505.
(180) Song, C.; Martínez, T. J. Atomic orbital based SOS-MP2 with tensor hypercontraction. I. GPU based tensor construction and exploiting sparsity. *J. Chem. Phys.* **2016**, *144*, 174111.
(181) Song, C.; Martínez, T. J. Atomic orbital based SOS-MP2 with tensor hypercontraction. II. Local tensor hypercontraction. *J. Chem. Phys.* **2017**, *146*, 034104.
(182) Watson, M. A.; Handy, N. C.; Cohen, A. J. Density functional calculations, using Slater basis sets, with exact exchange. *J. Chem. Phys.* **2003**, *119*, 6475−6481.
(183) Merlot, P.; Kjærgaard, T.; Helgaker, T.; Lindh, R.; Aquilante, F.; Reine, S.; Pedersen, T. B. Attractive electron-electron interactions within robust local fitting approximations. *J. Comput. Chem.* **2013**, *34*, 1486−1496.
(184) Mejía-Rodríguez, D.; Köster, A. M. Robust and efficient variational fitting of Fock exchange. *J. Chem. Phys.* **2014**, *141*, 124114.
(185) Hollman, D. S.; Schaefer, H. F.; Valeev, E. F. Semi-exact concentric atomic density fitting: Reduced cost and increased accuracy compared to standard density fitting. *J. Chem. Phys.* **2014**, *140*, 064109.
(186) Ihrig, A. C.; Wieferink, J.; Zhang, I. Y.; Ropo, M.; Ren, X.; Rinke, P.; Scheffler, M.; Blum, V. Accurate localized resolution of identity approach for linear-scaling hybrid density functionals and for many-body perturbation theory. *New J. Phys.* **2015**, *17*, 093020.
(187) Manzer, S. F.; Epifanovsky, E.; Head-Gordon, M. Efficient implementation of the pair atomic resolution of the identity approximation for exact exchange for hybrid and range-separated density functionals. *J. Chem. Theory Comput.* **2015**, *11*, 518−527.
(188) Rebolini, E.; Izsák, R.; Reine, S. S.; Helgaker, T.; Pedersen, T. B. Comparison of Three Efficient Approximate Exact-Exchange Algorithms: The Chain-of-Spheres Algorithm, Pair-Atomic Resolution-of-the-Identity Method, and Auxiliary Density Matrix Method. *J. Chem. Theory Comput.* **2016**, *12*, 3514−3522.
(189) Wirz, L. N.; Reine, S. S.; Pedersen, T. B. On Resolution-of-the-Identity Electron Repulsion Integral Approximations and Variational Stability. *J. Chem. Theory Comput.* **2017**, *13*, 4897−4906.
(190) Van Lenthe, E.; Baerends, J. E. Optimized Slater-type basis sets for the elements 1−118. *J. Comput. Chem.* **2003**, *24*, 1142−1156.
(191) Manby, F. R. Density fitting in second-order linear-r12 Møller-Plesset perturbation theory. *J. Chem. Phys.* **2003**, *119*, 4607−4613.
(192) Reeves, C. M.; Harrison, M. C. Use of gaussian functions in the calculation of wavefunctions for small molecules. II. The ammonia molecule. *J. Chem. Phys.* **1963**, *39*, 1−10.
(193) Harrison, J. F. Some one-electron properties of H2O and NH3. *J. Chem. Phys.* **1967**, *47*, 2990−2996.

https://dx.doi.org/10.1021/acs.jctc.9b00854
J. Chem. Theory Comput. 2020, 16, 875−891

(194) Gordon, M. S.; Binkley, J. S.; Pople, J. A.; Pietro, W. J.; Hehre, W. J. Self-Consistent Molecular-Orbital Methods. 22. Small Split-Valence Basis Sets for Second-Row Elements. *J. Am. Chem. Soc.* **1982**, *104*, 2797−2803.
(195) Takatsuka, A.; Ten-no, S.; Hackbusch, W. Minimax approximation for the decomposition of energy denominators in Laplace-transformed Møller−Plesset perturbation theories. *J. Chem. Phys.* **2008**, *129*, 044112.
(196) Helmich-Paris, B.; Visscher, L. Improvements on the minimax algorithm for the Laplace transformation of orbital energy denominators. *J. Comput. Phys.* **2016**, *321*, 927−931.
(197) Gerenkamp, M.; Grimme, S. Spin-component scaled second-order Møller-Plesset perturbation theory for the calculation of molecular geometries and harmonic vibrational frequencies. *Chem. Phys. Lett.* **2004**, *392*, 229−235.
(198) Grimme, S. Accurate calculation of the heats of formation for large main group compounds with spin-component scaled MP2 methods. *J. Phys. Chem. A* **2005**, *109*, 3067−3077.
(199) Fink, R. F. Spin-component-scaled Møller - Plesset (SCS-MP) perturbation theory: A generalization of the MP approach with improved properties. *J. Chem. Phys.* **2010**, *133*, 174113.
(200) Jung, Y.; Head-Gordon, M. A fast correlated electronic structure method for computing interaction energies of large van der Waals complexes applied to the fullerene-porphyrin dimer. *Phys. Chem. Chem. Phys.* **2006**, *8*, 2831−2840.
(201) Lochan, R. C.; Head-Gordon, M. Orbital-optimized opposite-spin scaled second-order correlation: An economical method to improve the description of open-shell molecules. *J. Chem. Phys.* **2007**, *126*, 164101.
(202) Kozuch, S.; Martin, J. M. Spin-component-scaled double hybrids: An extensive search for the best fifth-rung functionals blending DFT and perturbation theory. *J. Comput. Chem.* **2013**, *34*, 2327−2344.
(203) Ayala, P. Y.; Scuseria, G. E. Atom pair partitioning of the correlation energy. *Chem. Phys. Lett.* **2000**, *322*, 213−218.
(204) Kokkila Schumacher, S. I.; Hohenstein, E. G.; Parrish, R. M.; Wang, L. P.; Martínez, T. J. Tensor Hypercontraction Second-Order Møller-Plesset Perturbation Theory: Grid Optimization and Reaction Energies. *J. Chem. Theory Comput.* **2015**, *11*, 3042−3052.
(205) Jackson, J. D. *Classical electrodynamics*, 3rd ed.; John Wiley & Sons: New York, 1999.
(206) te Velde, G.; Bickelhaupt, F. M.; Baerends, E. J.; Fonseca Guerra, C.; van Gisbergen, S.; Snijders, J. G.; Ziegler, T. Chemistry with ADF. *J. Comput. Chem.* **2001**, *22*, 931−967.
(207) *ADF2018*; SCM, Theoretical Chemistry, Vrije Universiteit: Amsterdam, The Netherlands, https://www.scm.com.
(208) Franchini, M.; Philipsen, P. H. T.; Van Lenthe, E.; Visscher, L. Accurate Coulomb potentials for periodic and molecular systems through density fitting. *J. Chem. Theory Comput.* **2014**, *10*, 1994−2004.
(209) Franchini, M.; Philipsen, P. H. T.; Visscher, L. The becke fuzzy cells integration scheme in the amsterdam density functional program suite. *J. Comput. Chem.* **2013**, *34*, 1819−1827.
(210) Hu, X.; Yang, W. Accelerating self-consistent field convergence with the augmented Roothaan-Hall energy function. *J. Chem. Phys.* **2010**, *132*, 054109.
(211) Boys, S. F.; Bernardi, F. The calculation of small molecular interactions by the differences of separate total energies. Some procedures with reduced errors. *Mol. Phys.* **1970**, *19*, 553−566.
(212) Van Lenthe, E.; Baerends, E. J.; Snijders, J. G. Relativistic regular two-component hamiltonians. *J. Chem. Phys.* **1993**, *99*, 4597.
(213) Van Lenthe, E.; Baerends, E. J.; Snijders, J. G. Relativistic total energy using regular approximations. *J. Chem. Phys.* **1994**, *101*, 9783−9792.
(214) Van Lenthe, E.; Snijders, J. G.; Baerends, E. J. The zero-order regular approximation for relativistic effects: The effect of spin-orbit coupling in closed shell molecules. *J. Chem. Phys.* **1996**, *105*, 6505−6516.
(215) Van Lenthe, E.; Ehlers, A.; Baerends, J. E. Geometry optimizations in the zero order regular approximation for relativistic effects. *J. Chem. Phys.* **1999**, *110*, 8943−8953.
(216) Source code available on https://github.com/bhelmichparis/laplace-minimax.
(217) Rezac, J.; Riley, K. E.; Hobza, P. S66: A well-balanced database of benchmark interaction energies relevant to biomolecular structures. *J. Chem. Theory Comput.* **2011**, *7*, 2427−2438.
(218) Goerigk, L.; Grimme, S. A thorough benchmark of density functional methods for general main group thermochemistry, kinetics, and noncovalent interactions. *Phys. Chem. Chem. Phys.* **2011**, *13*, 6670−6688.
(219) Grimme, S.; Antony, J.; Ehrlich, S.; Krieg, H. A consistent and accurate ab initio parametrization of density functional dispersion correction (DFT-D) for the 94 elements H-Pu. *J. Chem. Phys.* **2010**, *132*, 154104.
(220) Sedlak, R.; Janowski, T.; Pitoňák, M.; Řezáč, J.; Pulay, P.; Hobza, P. Accuracy of quantum chemical methods for large noncovalent complexes. *J. Chem. Theory Comput.* **2013**, *9*, 3364−3374.
(221) Cremer, D. Møller-Plesset perturbation theory: From small molecule methods to methods for thousands of atoms. *Wiley Interdiscip. Rev. Comput. Mol. Sci.* **2011**, *1*, 509−530.
(222) Metz, B.; Stoll, H.; Dolg, M. Small-core multiconfiguration-Dirac-Hartree-Fock-adjusted pseudopotentials for post-d main group elements: Application to PbH and PbO. *J. Chem. Phys.* **2000**, *113*, 2563−2569.
(223) Peterson, K. A.; Figgen, D.; Goll, E.; Stoll, H.; Dolg, M. Systematically convergent basis sets with relativistic pseudopotentials. II. Small-core pseudopotentials and correlation consistent basis sets for the post-d group 16−18 elements. *J. Chem. Phys.* **2003**, *119*, 11113−11123.
(224) Sure, R.; Grimme, S. Comprehensive Benchmark of Association (Free) Energies of Realistic Host-Guest Complexes. *J. Chem. Theory Comput.* **2015**, *11*, 3785−3801.
(225) Jones, T. C.; Sementa, L.; Stener, M.; Gagnon, K. J.; Thanthirige, V. D.; Ramakrishna, G.; Fortunelli, A.; Dass, A. Au21S(SAdm)15: Crystal Structure, Mass Spectrometry, Optical Spectroscopy, and First-Principles Theoretical Analysis. *J. Phys. Chem. C* **2017**, *121*, 10865−10869.
(226) Weigend, F.; Köhn, A.; Hättig, C. Efficient use of the correlation consistent basis sets in resolution of the identity MP2 calculations. *J. Chem. Phys.* **2002**, *116*, 3175−3183.
(227) Hättig, C. Optimization of auxiliary basis sets for RI-MP2 and RI-CC2 calculations: Core-valence and quintuple-ζ basis sets for H to Ar and QZVPP basis sets for Li to Kr. *Phys. Chem. Chem. Phys.* **2005**, *7*, 59−66.
(228) Hill, J. G.; Platts, J. A. Auxiliary basis sets for density fitting-MP2 calculations: Nonrelativistic triple- all-electron correlation consistent basis sets for the 3d elements Sc-Zn. *J. Chem. Phys.* **2008**, *128*, 044104.
(229) Caldeweyher, E.; Bannwarth, C.; Grimme, S. Extension of the D3 dispersion coefficient model. *J. Chem. Phys.* **2017**, *147*, 034112.
(230) Caldeweyher, E.; Ehlert, S.; Hansen, A.; Neugebauer, H.; Spicher, S.; Bannwarth, C.; Grimme, S. A generally applicable atomic-charge dependent London dispersion correction. *J. Chem. Phys.* **2019**, *150*, 154122.
(231) Stefan, G.; Stephan, E.; Lars, G. Effect of the damping function in dispersion corrected density functional theory. *J. Comput. Chem.* **2011**, *32*, 1456−1465.
(232) Smith, D. G.; Burns, L. A.; Patkowski, K.; Sherrill, C. D. Revised Damping Parameters for the D3 Dispersion Correction to Density Functional Theory. *J. Phys. Chem. Lett.* **2016**, *7*, 2197−2203.

https://dx.doi.org/10.1021/acs.jctc.9b00854
J. Chem. Theory Comput. 2020, 16, 875−891